$\pi^- p$ charge-exchange amplitude zeros from a Barrelet analysis between 1.4 and 2.3 GeV

D. M. Chew*
Lawrence Berkeley Laboratory, University of California, Berkeley, California 94720
(Received 6 December 1977)

Using the available scattering and polarization pion-nucleon charge-exchange data, we have performed a Barrelet-moment analysis between 1.4 and 2.3 GeV. The method allows us to identify and discard data with important systematic error. Above 1.5 GeV, ten zeros are unambiguously required in order to represent the retained data. An attempt is made to resolve the discrete ambiguity and to obtain the location of amplitude zeros close to the physical region.

I. INTRODUCTION

Data on the charge-exchange reaction[1,2]

$$\pi^- p \to \pi^0 n \tag{1}$$

constitute an important supplement to elastic $\pi^{\pm} p$ data, since isospin invariance relates the charge-exchange amplitude to the difference of the two elastic amplitudes. The recent availability of accurate charge-exchange data makes it possible to check amplitude analyses that have been based on elastic data alone.[3] These checks have revealed alarming discrepancies.[4] Either the recent charge-exchange measurements are grossly in error, or currently accepted elastic amplitudes based on partial-wave analysis possess serious deficiencies. As part of a Barrelet-zero approach to πN amplitude analysis,[5,6] which we hope will lead to more reliable conclusions than have been reached by the partial-wave route, we lay the groundwork in this paper for a direct determination of the charge-exchange amplitude.

For reasons explained elsewhere, amplitude analysis through Barrelet moments and Barrelet zeros[7] is less subjective than conventional partial-wave analysis in conjunction with least-square polynomial fitting. The Barrelet method, furthermore, by objectively generating moments from *individual* experiments, is capable of revealing systematic error.[8] In this paper, we report the results of Barrelet-moment analysis for available charge-exchange data in the interval $0.6 < P_{\text{lab}} < 2.5$ GeV/c ($1.4 < E_{\text{c.m.}} < 2.3$ GeV).[9] After eliminating certain data which have large statistical errors, or which our results suggest possess a systematic error larger than the stated statistical error, we determine the trajectories of the Barrelet zeros that come sufficiently close to the physical region to be detected. The discrete ambiguity is handled by the method that has been used earlier for elastic data.[5,6]

We do not discuss in this paper the determination of the charge-exchange amplitude in terms of zeros, or the comparison with the difference of $\pi^- p$ and $\pi^+ p$ elastic amplitudes. These steps will be reported in a later paper.

II. METHOD OF ANALYSIS

Barrelet developed his method[7] for use with individual experiments that each cover a finite portion of the physical angular interval $a < \cos < b$. In this interval, the differential cross section is represented by a superposition of orthonormal pseudopolynomials $p_l(\cos\theta)$,

$$\frac{d\sigma}{d\Omega} \simeq \sum_{l=0}^{l=N_1} A_l p_l(\cos\theta) . \tag{2}$$

The pseudopolynomials are defined with respect to a weighting norm $n_p(\cos\theta)$ such that

$$\int_a^b d(\cos\theta) p_l(\cos\theta) p_{l'}(\cos\theta) n_p(\cos\theta) = \delta_{ll'} , \tag{3}$$

where the moments A_l are calculated from the formula

$$A_l = \int_a^b \frac{d\sigma}{d\Omega} (\cos\theta) p_l(\cos\theta) n_p(\cos\theta) d(\cos\theta) . \tag{4}$$

With data sufficiently dense in $\cos\theta$, the latter quadrature, when carried out with care,[10] allows translation of the statistical error on individual data points into statistical errors for the moments A_l. Barrelet chooses the truncation point N_1 of the polynomial expansion on the basis that A_l is theoretically expected to tend smoothly toward zero for l sufficiently large.[11] As soon as the error in the moments begins to overlap zero, Barrelet terminates the expansion in Eq. (2); to go further is statistically meaningless. The parameter N_1 is determined by the data, not guessed. For spin-0–spin-$\frac{1}{2}$ elastic scattering where the polarization P can be measured, one may make a similar analysis of $P\, d\sigma/d\Omega$, leading to a second set of moments B_l with $l < N_2$.

The weighting norm is to be chosen so as to give comparable weight to all data points in the

calculation of the moments.[8,12] In the case of the charge-exchange data, we take n_p equal to 1. A major advantage of the Barrelet method of data analysis is that Barrelet's truncation points N_1 and N_2 are objectively fixed by the statistical errors. The polynomial fit arrived at through formulas (2) and (4) contains all the information in the data. It takes into account information due to either low statistics (which reflect into the errors on the moments) or systematic errors larger than the statistical errors (which affect the asymptotic behavior of the moments), as explained in the following section.[13]

III. SELECTION OF DATA

We have considered the results of all charge-exchange differential cross-section experiments

TABLE I. (a). Characteristics of charge-exchange scattering data (Ref. 1) and maximum statistically significant order N_1. (b). Characteristics of charge-exchange polarization (Ref. 2) and value of maximum statistically significant order N.

	(a)						(b)				
	P_{lab} (GeV/c)	Ref.	No. pts.	cosθ interval[a]	N_1		P_{lab} (GeV/c)	Ref.	No. pts.	cosθ interval	N
1	0.618	B76	27	−0.96/1.0	7	1	0.617	B76	17	−0.70/0.95	7
2	0.624	C67	20	−1.0 /1.0	4	2	0.675	B76	20	−1.0 /0.95	13
3	0.658	C67	20	−1.0 /1.0	4	3	0.723	B76	20	−1.0 /0.95	9
4	0.675	B76	30	−0.96/1.0	13	4	0.776	B76	20	−1.0 /0.95	11
5	0.718	C67	20	−1.0 /1.0	4	5	0.827	B76	20	−1.0 /0.95	12
6	0.724	B76	31	−0.96/1.0	11	6	0.974	B76	20	−1.0 /0.95	13
7	0.776	B76	31	−0.96/1.0	11	7	1.027	B76	20	−1.0 /0.95	12
8	0.782	C67	20	−1.0 /1.0	5	8	1.030	S74	20	−0.92/0.78	11
9	0.825	B76	31	−0.96/1.0	12	9	1.076	B76	20	−1.0 /0.95	13
10	0.832	C67	20	−1.0 /1.0	5	10	1.170	B76	19	−1.0 /0.95	11
11	0.974	B76	34	−0.96/1.0	13	11	1.245	S74	19	−0.84/0.80	6
12	1.004	C67	20	−1.0 /1.0	5	12	1.274	B76	20	−1.0 /0.95	13
13	1.027	B76	31	−0.96/1.0	12	13	1.355	B76	19	−1.0 /0.95	8
14	1.030	N72	87(88)	−0.85/1.0[a]	13	14	1.437	B76	20	−1.0 /0.95	9
15	1.060	B64	20	−1.0 /1.0	2	15	1.440	S74	20	−0.90/0.81	9
16	1.077	B76	32	−0.96/0.94	9	16	1.505	B76	20	−1.0 /0.95	9
17	1.105	C67	20	−1.0 /1.0	7	17	1.590	S74	20	−0.90/0.81	8
18	1.170	B76	33	−0.96/0.96	11	18	1.600	B76	20	−1.0 /0.95	8
19	1.248	C67	20	−1.0 /1.0	7	19	1.687	B76	20	−1.0 /0.95	11
20	1.275	B76	33	−0.96/0.96	13	20	1.767	B76	20	−1.0 /0.95	8
21	1.356	B76	31	−0.96/0.94	9	21	1.790	S74	19	−0.81/0.82	8
22	1.432	C67	20	−1.0 /1.0	7	22	1.871	B76	20	−1.0 /0.95	10
23	1.438	B76	33	−0.96/0.96	13	23	1.975	B76	19	−1.0 /0.95	10
24	1.505	B76	33	−0.96/0.96	11	24	2.055	B76	19	−1.0 /0.95	11
25	1.590	N72	91(93)	−0.85/1.0[a]	9	25	2.267	B76	17	−1.0 /0.95	12
26	1.601	B76	33	−0.96/0.96	10						
27	1.688	B76	34	−0.96/0.96	12						
28	1.715	C69	40	−1.0 /1.0	4						
29	1.767	B76	34	−0.96/0.96	8						
30	1.790	N72	87(88)	−0.85/1.0[a]	7						
31	1.872	B76	34	−0.96/0.96	13						
32	1.889	C69	40	−1.0 /1.0	7						
33	1.975	B76	34	−0.96/0.96	10						
34	1.990	N72	73(75)	−0.85/1.0[a]	10						
35	2.056	B76	34	−0.96/0.96	12						
36	2.071	C69	40	−1.0 /1.0	5						
37	2.190	N72	70(72)	−0.85/1.0[a]	5						
38	2.265	C69	40	−1.0 /1.0	11						
39	2.267	B76	35	−0.96/0.96	12						
40	2.390	N72	63(66)	−0.85/1.0[a]	10						
41	2.460	C69	40	−1.0 /1.0	11						

[a] As explained in N72, data in the very backward direction ($-1 < \cos\theta < -0.85$), where the chamber efficiency is low, have been omitted because of the systematic error in the correction which is large and the method of moments cannot be applied (see Ref. 10).

where measurements were made for at least 20 different angles (at each energy). Columns 2, 4, and 5 of Table I list the characteristics of each of 41 different experiments. A sequence of Barrelet moments was determined for each experiment[14,15] according to the prescription of Sec. II above; the sequence is terminated when two successive moments both have statistical errors that overlap zero. For data where the systematic error is smaller than the statistical error, the upper limit N_1 so defined (listed in column 6) coincides with the maximum-order moment that is significant. At a given energy, the relative statistical accuracy of different experiments is measured by N_1, so we may use low relative values of this parameter as an objective basis for eliminating data. This criterion leads us to discard immediately the results[1] from C67, B64, and C69.[16]

Although Barrelet-moment analysis was not designed to deal with systematic error, we may use it to identify experiments that contain significant systematic aberations—as we now explain. For data where the error is predominantly statistical, one expects the goodness of fit achieved by the Barrelet polynomial representation of formula (2) to increase with the order of the polynomial up to the limit N_1. The expansion coefficients (moments) are theoretically supposed to decrease exponentially (see Ref. 11), so we expect to see the χ^2 per data point fall smoothly to the neighborhood of 1 as the polynomial order approaches N_1; thereafter the goodness of fit should not change significantly. Polynomials of an order higher than N_1 are not physically meaningful—corresponding merely to statistical fluctuations in the data—but their inclusion should not suddenly spoil the goodness of the overall fit.

Suppose, on the other hand, that there is a small proportion of data points with large systematic error. These points are (more or less) ignored by

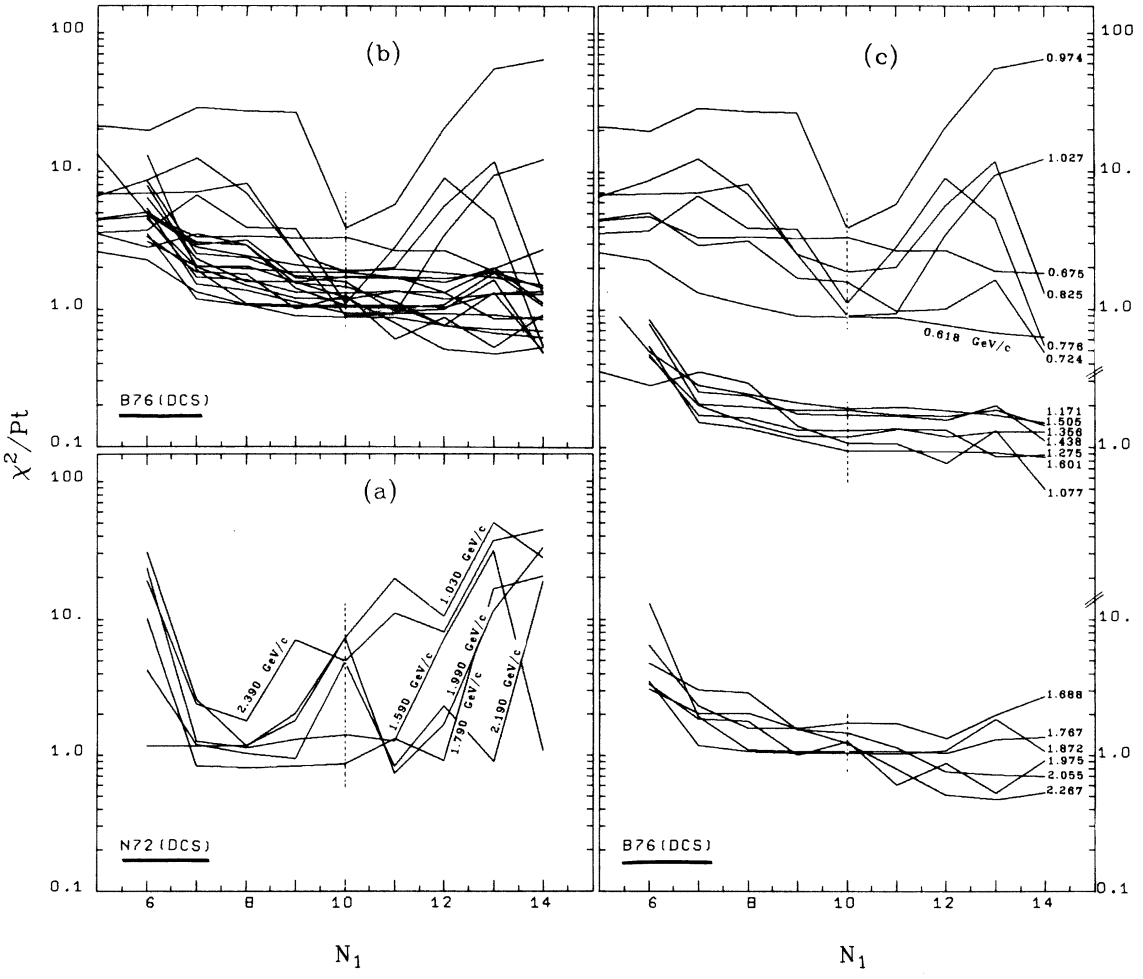

FIG. 1. χ^2 per data point vs the polynomial order N_1 for the scattering data N72 (a) and B76 (b), detailed in (c).

moments of low order but seriously influence the value of appropriately high-order moments. Inclusion of such high-order moments may upset the overall goodness of fit. Systematic error is thus signaled by a χ^2 per data point that rises (or fluctuates) significantly in the neighborhood of N_1 *after* a minimum has been achieved. An even more obvious signal is the absence of any smooth tendency for the χ^2 per point to approach the value of 1.

Figure 1 shows the χ^2 per data point as a function of polynomial order at each B76 and N72 energy. We are led by such considerations to believe that serious systematic errors exist in the N72 data at all of the six different energies where measurements were made [Fig. 1(a)]. As explained later, the maximum statistically significant order is ~10. We do not include any of the N72 data in the remainder of our analysis. Similar considerations lead us to discard, in principle, B76 data at four neighboring energies, $P_{1ab} = 0.776$, 0.825, 0.974, and 1.027 GeV/c [Figs. 1(b), and 1(c) for detail] and the last two energies of C69. The degree of disagreement between the N72 and B76 data is indicated in Fig. 2, where we compare at the same energy the 10-th order polynomial representation of B76 with the data of N72 and its polynomial representation of order 6 [Fig. 1(a)] and 10 [Figs. 1(b), 1(c), and 1(d)].

Some check on our selection of data can be achieved by comparing two independent pieces of information on forward and backward differential cross sections. Our extrapolation of the differential cross section to 0° and 180° of B76 for $N_1 = 10$ are plotted in Figs. 3(a) and 3(b), where the indicated error is the largest deviation between the $N_1 = 10$ extrapolation and the extrapolation for any other order whose χ^2 value differs from that for $N_1 = 10$ by less than one unit. We show in Fig. 3(a) the forward differential cross section as determined from $\pi^{\pm} p$ total cross sections and dispersion relations.[17] A uniform shift of about 10% in our extrapolated values would bring agreement. If the problem is only a matter of overall normalization of the scattering data, there will be no effect on the positions of Barrelet zeros. Direct high-precision measurements of $d\sigma/d\Omega$ at 180° have been made[18] and are compared with our extrapolations

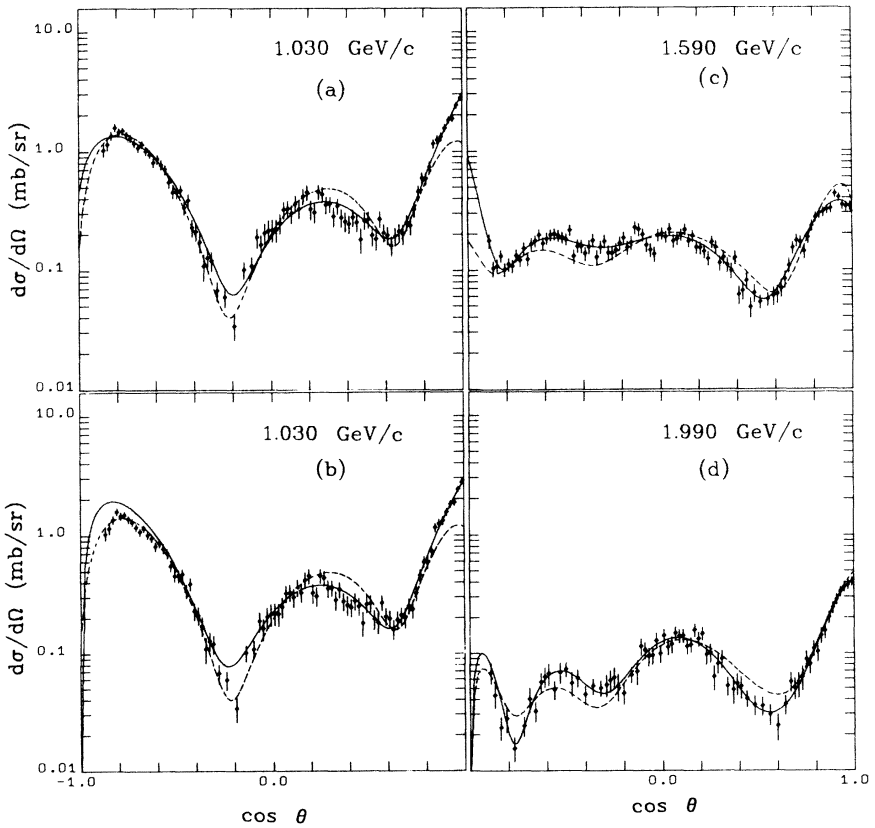

FIG. 2. Comparison of the polynomial representation of the B76 scattering data ($N_1 = 10$, dotted line) with N72 data and polynomial representation thereof [(a) $N_1 = 6$ and (b), (c), (d) $N_1 = 10$, solid line] at three closely matched energies. (The data of B76 are in Fig. 6.)

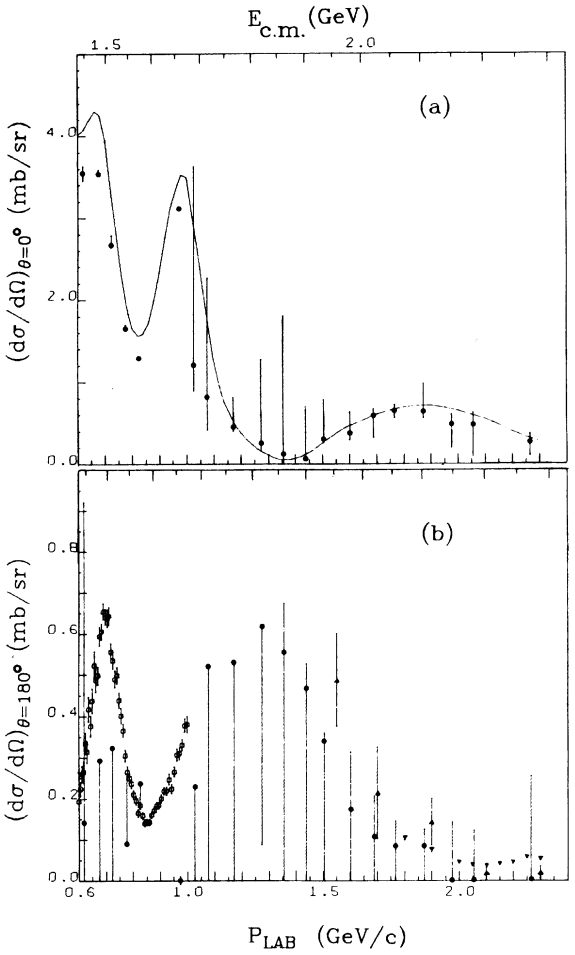

FIG. 3. (a) $(d\sigma/d\Omega)_{\theta=0}$ from extrapolation of the polynomial representation of B76 scattering data. The line is the value calculated in Ref. 17. (b) $(d\sigma/d\Omega)_{\theta=180}$ for extrapolation of the polynomial representation of B76 scattering data, compared with the data of Ref. 18, (□) for D75, (△) for A69, and (▽) for K72.

in Fig. 3(b). A significant discrepancy with D75 appears at $P_{\rm lab} \sim 0.700$ GeV/c, but we understand[19] that the authors of D75 now believe their measurement may have contained substantial systematic error. Above 1.5 GeV/c we find ourselves in agreement with A68 and K72. No direct data exist for $1.0 < P_{\rm lab} < 1.5$ GeV/c with which to compare our extrapolations.

The second half of Table I lists the available polarization data—two experiments, B76 and S74, being included. Superficial comparison of the data immediately reveals an energy, corresponding to $P_{\rm lab} = 1.03$ GeV/c, where the two experiments qualitatively disagree in the backward direction, B76 giving a positive polarization and S74 a negative. Because backward direction polarization is here varying rapidly with energy (see the B76 data), an error in the beam momentum of one of the experiments by 20 or 30 MeV/c could account for the discrepancy.

Momentarily ignoring this difficulty, it is straightforward to make a Barrelet-moment analysis of $P\,d\sigma/d\Omega$ at those energies where both P and $d\sigma/d\Omega$ data have been taken and to examine the goodness of fit as a function of polynomial order, exactly as we did above for $d\sigma/d\Omega$. However, for the Barrelet-zero determination of the amplitude $F(s,w)$ it is necessary to consider the experimental quality $\Sigma(w)$, where $w = e^{i\theta}$ and

$$\Sigma(w) = \Sigma^+ = \frac{d\sigma}{d\Omega}(1+P), \quad 0 < \theta < \pi, \tag{5}$$

$$\Sigma(w) = \Sigma^- = \frac{d\sigma}{d\Omega}(1-P), \quad \pi < \theta < 2\pi, \tag{6}$$

so we shall treat the polarization data via the Barrelet-moment analysis of $\Sigma(w)$ with respect at pseudopolynomials in the variable w.[7] (Polynomials in $\cos\theta$ are pseudopolynomials in w.) The maximum significant order N is set by the smaller of the two separate truncation points N_1, N_2. This maximum order will limit the number of zeros that can be determined from the data (and eventually the number of different partial waves.) Because polarization measurements are less accurate than differential cross sections, it is generally N_2 that sets the limit, i.e., $N = N_2$. The angular interval, furthermore, is the smaller of the intervals covered in the separate measurements of P and $d\sigma/d\Omega$.

Our approach then is to combine data on P and $d\sigma/d\Omega$ so as to generate moments of $\Sigma(w)$ and corresponding pseudopolynomial representations of $\Sigma^+(w)$ and $\Sigma^-(w)$ $[= \Sigma^+(\bar{w})]$. Representations of $d\sigma/d\Omega$ and P may be obtained from

$$\frac{d\sigma}{d\Omega} = \tfrac{1}{2}(\Sigma^+ + \Sigma^-), \tag{7}$$

$$P = \frac{\Sigma^+ - \Sigma^-}{\Sigma^+ + \Sigma^-}. \tag{8}$$

Because of the linearity of the relations (5), (6), and (7), the polynomial representation of $d\sigma/d\Omega$ is affected by the polarization data only to the extent that the angular interval may be contracted and the value of N reduced.

In the absence of systematic errors, the behavior of the goodness of fit (χ^2 per point) for *both* $d\sigma/d\Omega$ and P should be as described above for $d\sigma/d\Omega$. Figure 4 shows the χ^2 per point as a function of polynomial order N for the B76 scattering and polarization data within a common angular interval. Notice—in Fig. 4(a)—that the $d\sigma/d\Omega$ behavior is similar to that of Fig 1(b)—the same four

neighboring energies exhibiting evidence of a systematic error larger than the statistical error. The polarization χ^2 per point in Fig. 4(b), reveals no such strong evidence.

The degree of disagreement between B76 and S74 polarization measurements is indicated in Fig. 5 where we compare our different polynomial approximations to S74 with the closest-energy (within 10 MeV) order-10 polynomial approximation to B76. Due to the fact that (1) we find no evidence for large systematic error in the B76 polarization measurements, (2) the polarization statistical errors are larger for S74 than B76, and (3) the angular interval covered is smaller in S74 than in B76, we henceforth disregard the S74 polarization data. The choice $N=10$ will now be discussed.

IV. DETERMINATION OF THE NUMBER OF STABLE ZEROS

It turns out, both from an examination of Table I and from the original Barrelet criterion, that N varies between 7 and 13 at the different energies under consideration. At the highest energies the variation is between 8 and 12. Changing N by 1 or 2 units at a given energy does not strongly alter the goodness of the polynomial fit[20] (see Fig. 4), but there may be an important alteration in the location of some of the zeros of $\Sigma(w)$. A stable zero is one whose position does not drastically change when the order of the polynomial is changed. It was shown by Barrelet that stable zeros are near the physical region (the unit circle in the complex w plane), so instability means a large uncertainty in the zero's position.

Analysis of the πN elastic scattering has con-

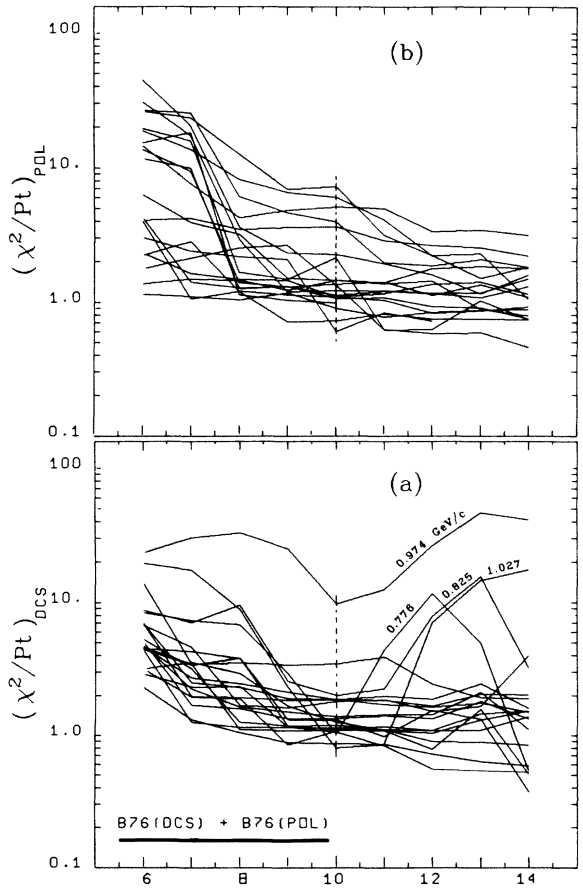

FIG. 4. χ^2 per data point versus polynomial order N when B76 scattering and polarization data are simultaneously analyzed. (a) for $d\sigma/d\Omega$, (b) for P.

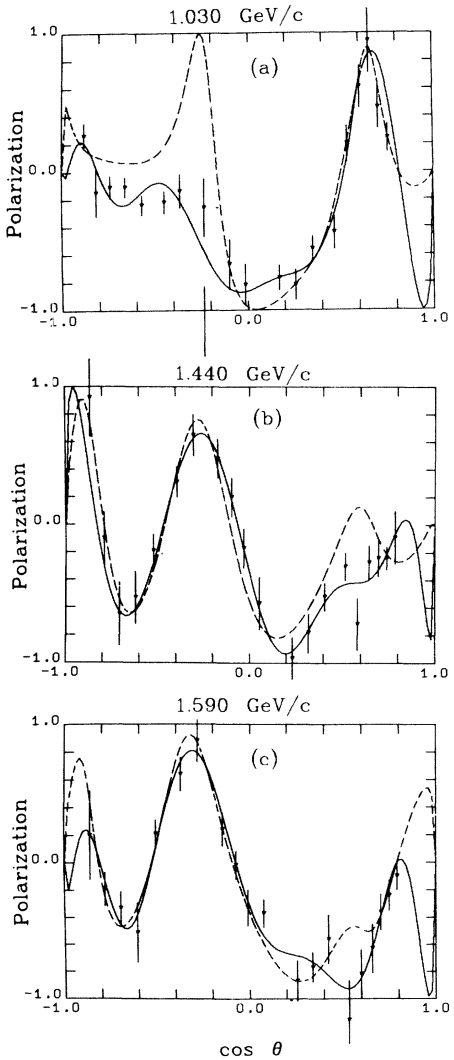

FIG. 5. Comparison of $N=10$ polynomial representation for P with S74 data at three closely matched energies, (a) 1.030 (S74) and 1.027 (B76), (b) 1.440 (S74) and 1.437 (B76), (c) 1.590 (S74) and 1.601 (B76). (The data of B76 is in Fig. 6.)

firmed the theoretically expected smooth behavior of the position of zeros as a function of energy, especially in intervals free from strong and sharp resonances. Zeros do not suddenly appear or disappear.[21] It has, furthermore, been shown that zeros occur in approximately complex-conjugate pairs, so one expects the total number of nearby zeros to be even. We have consequently examined the position of zeros for $N=6$, 8, 10, and 12 at each energy and looked for smoothness of position variation. The following results have emerged:

(a) At the two lowest energies, $P_{\text{lab}}=0.618$ and 0.675 GeV/c, the 6th-order polynomial has relatively stable roots corresponding roughly to the six nearby zeros labeled (A,H), (C,B), (E,F) in Table II and gives an acceptable value of χ^2 per point (1.85 and 3.25, respectively, versus 0.87 and 2.64 for the 10th-order polynomial at the same energies).

(b) At the next energy ($P_{\text{lab}}=0.724$ GeV/c), however, and most energies within our range, two additional pairs of stable zeros (within the disc of polynomial convergence) need to be accommodated. They are labeled (D,I) and (G,J).

Therefore, the minimum N that can handle the entire energy interval is $N=10$. Using $N=12$ does not anywhere significantly improve the goodness of the polynomial representation. The two extra zeros that appear when N is changed from 10 to 12 seem to represent a statistically meaningless "doubling" of two zeros already present. The pattern of doubling shows no consistency as the energy varies. Consequently, since both conditions—stability of the zeros at most energies within our energy range and a consistent pattern in the position of the zeros—are realized for $N=10$ (see Fig. 7, where the labels of Table II are displayed at $P_{\text{lab}}=1.438$ GeV/c) we have chosen to work uniformly with this value of N. Ten zeros are correspondingly deduced at each energy. At some energies, less than ten zeros are "stable" in the sense of Barrelet, this fact is exhibited by the failure of one or more zero positions to be securely (within errors)[22] located inside the disc of convergence. [More accurate date are needed for a better determination of their position, as can be observed from the data of Fig. 6, at the value of $\cos\theta=\mathrm{Re}\,z_i$ given in Table II.] The fact that already at $P_{\text{lab}}=0.724$ GeV/c all ten zeros are unambiguously stable is remarkable considering that in the available data[5,6] for π^+p scattering, ten zeros were not required until $P_{\text{lab}}=1.450$ GeV/c. Figure 6 shows the $N=10$ polynomial representations of the B76 data, the corresponding χ^2 per data point given by the dotted line on Fig. 6(a).

V. ZERO TRAJECTORIES

At each energy we have determined 11 moments of $\Sigma(w)$ and converted this information into the positions of ten zeros in the complex w plane. There is the usual discrete ambiguity between the location w_i and $\bar{w}_i^{-1}$, to which we devote attention in the following sections. In Fig. 7 we have presented our results at each energy, with the convention that all zeros lie outside the unit circle except for the two furthest ones from the physical regions (which would have to be drawn too far out of the plot). The inside boundary of the disc of convergence of the polynomial expansion is indicated, allowing identification of the nearby stable zeros.[23]

By comparing the positions of zeros at neighboring energies, where the relative displacements are moderate, it is possible to construct trajectories w_i in the complex w plane. The continuity of individual trajectories is nicely displayed by plotting $\mathrm{Re}\,t_i$ vs $\sqrt{s}$. The complete set of ten trajectories is thus shown in Fig. 8 and then two at a time with errors in Fig. 9. The five trajectories labeled A,C,E,G,I represent zeros of Σ^- (corresponding to polarization maxima) while those labeled B,D,F,H,J represent zeros of Σ^+ (polarization minima). Note that for such a plot the discrete ambiguity is irrelevant. On the same Fig. 9 are displayed also the ten trajectories in the complex w plane, with the errors for $|w_i|>1$. The two trajectories (D and I) that wander farthest from the physical region are poorly determined, but at certain energies even these zeros come close enough to produce extreme polarization at $\cos\theta=\mathrm{Re}\,z_i$. Table II lists the positions of these ten zeros (with the convention that they *all* lie outside the unit circle in the w plane) in different variables, with the radius of the outside boundary of the convergence disc, R_w.

VI. DETERMINATION OF THE CRITICAL POINTS

In an effort to resolve the discrete ambiguity, we need first to identify the critical points where trajectories cross the physical region, moving in the w complex plane from inside the unit circle to outside, or vice versa. Because $P=\pm1$ at a critical point, polarization measurements of high accuracy, closely spaced in energy, can settle this question. In practice, experimental inadequacies leave considerable uncertainty. Figure 10 plots $|w_i|$ for each zero (assumed outside the unit circle) in the w plane. Critical points occur at energies when the distance goes to zero, i.e., when $|w_i|=1$. If the statistical error on the measured polarization at such an energy is compatible with $P=\pm1$, we list the critical point in Table III

TABLE II. Zero locations of $\pi^- p$ charge-exchange data for $0.62 < P_{lab} < 2.7$ GeV/c, assuming all zeros to be outside the unit circle in the w plane, in different variables, z (=cosθ), t, and w. In the last column is the value of the outside boundary of the disk of convergence of the polynomial expansion, assuming the first singularity to be the ρ meson.

Traj.	P_{lab} (GeV/c)	$E_{c.m.}$ (GeV)	Rez	Imz	Ret [a] (GeV^2)	Imt (GeV^2)	Rew [b]	Imw [b]	Re[$\pm\delta(w)$] [b]		Im[$\pm\delta(w)$] [b]	
1A	0.618	1.445	0.273	−0.060	−0.234	−0.019	0.290	−1.024	0.066	0.126	1.064	5.502
1B	0.618	1.445	0.054	0.327	−0.305	0.105	0.070	1.378	0.082	0.103	1.379	5.502
1C	0.618	1.445	−0.682	−0.214	−0.541	−0.069	−0.868	−0.998	0.209	0.226	1.323	5.502
1D	0.618	1.445	1.098	0.094	0.032	0.030	1.590	0.305	0.270	0.112	1.619	5.502
1E	0.618	1.445	−0.990	−0.031	−0.641	−0.010	−1.138	−0.236	0.166	0.160	1.162	5.502
1F	0.618	1.445	−0.493	0.162	−0.481	0.052	−0.583	1.051	0.089	0.084	1.202	5.502
1G	0.618	1.445	0.817	−0.232	−0.059	−0.075	1.095	−0.913	0.124	0.105	1.425	5.502
1H	0.618	1.445	0.764	0.343	−0.076	0.110	1.092	1.144	0.151	0.142	1.581	5.502
1I	0.618	1.445	−0.302	−0.327	−0.419	−0.105	−0.399	−1.340	0.281	0.225	1.398	5.502
1J	0.618	1.445	−0.859	0.063	−0.599	0.020	−0.962	0.589	0.075	0.079	1.128	5.502
2A	0.675	1.481	0.386	−0.194	−0.225	−0.071	0.465	−1.140	0.088	0.088	1.231	5.044
2B	0.675	1.481	0.014	0.349	−0.361	0.128	0.018	1.409	0.079	0.122	1.409	5.044
2C	0.675	1.481	−0.602	−0.139	−0.586	−0.051	−0.705	−0.956	0.076	0.084	1.188	5.044
2D	0.675	1.481	1.138	0.128	0.051	0.047	1.723	0.378	0.454	0.236	1.764	5.044
2E	0.675	1.481	−0.976	−0.024	−0.723	−0.009	−1.074	−0.265	0.285	0.081	1.107	5.044
2F	0.675	1.481	−0.439	0.137	−0.526	0.050	−0.505	1.048	0.052	0.054	1.163	5.044
2G	0.675	1.481	0.916	−0.324	−0.031	−0.118	1.354	−1.001	0.376	0.209	1.684	5.044
2H	0.675	1.481	0.767	0.412	−0.085	0.151	1.139	1.261	0.265	0.162	1.700	5.044
2I	0.675	1.481	−0.127	−0.277	−0.412	−0.101	−0.161	−1.308	0.143	0.147	1.317	5.044
2J	0.675	1.481	−0.884	0.181	−0.689	0.066	−1.163	0.755	0.209	0.102	1.386	5.044
3A	0.724	1.511	0.206	−0.160	−0.321	−0.065	0.239	−1.152	0.086	0.086	1.176	4.722
3B	0.724	1.511	−0.011	0.330	−0.409	0.133	−0.014	1.382	0.093	0.099	1.382	4.722
3C	0.724	1.511	−0.396	−0.135	−0.564	−0.055	−0.454	−1.065	0.051	0.060	1.158	4.722
3D	0.724	1.511	1.102	0.019	0.041	0.008	1.567	0.065	0.195	0.147	1.568	4.722
3E	0.724	1.511	−1.028	−0.029	−0.819	−0.012	−1.288	−0.142	0.282	0.206	1.296	4.722
3F	0.724	1.511	−0.413	0.148	−0.571	0.060	−0.479	1.073	0.060	0.062	1.175	4.722
3G	0.724	1.511	0.688	−0.298	−0.126	−0.121	0.937	−1.122	0.181	0.141	1.462	4.722
3H	0.724	1.511	0.788	0.320	−0.086	0.129	1.117	1.088	0.111	0.084	1.559	4.722
3I	0.724	1.511	−0.344	−1.351	−0.543	−0.546	−0.623	−3.019	2.568	3.052	3.083	4.722
3J	0.724	1.511	−0.912	0.070	−0.773	0.028	−1.057	0.510	0.128	0.166	1.173	4.722
4A	0.776	1.543	0.443	−0.192	−0.248	−0.085	0.535	−1.113	0.067	0.073	1.235	4.436
4B	0.776	1.543	−0.041	0.279	−0.464	0.124	−0.052	1.316	0.085	0.061	1.317	4.436
4C	0.776	1.543	−0.189	−0.153	−0.530	−0.068	−0.218	−1.148	0.064	0.044	1.168	4.436
4D	0.776	1.543	1.077	0.101	0.034	0.045	1.531	0.341	0.190	0.125	1.568	4.436
4E	0.776	1.543	−1.006	−0.004	−0.894	−0.002	−1.121	−0.044	0.216	0.127	1.122	4.436
4F	0.776	1.543	−0.487	0.257	−0.662	0.115	−0.623	1.178	0.184	0.156	1.333	4.436
4G	0.776	1.543	0.859	−0.215	−0.063	−0.096	1.152	−0.844	0.122	0.107	1.428	4.436
4H	0.776	1.543	0.728	0.294	−0.121	0.131	0.997	1.088	0.077	0.072	1.476	4.436
4I	0.776	1.543	−0.564	−0.640	−0.697	−0.285	−0.893	−1.735	0.345	0.653	1.951	4.436
4J	0.776	1.543	−0.933	0.079	−0.861	0.035	−1.112	0.489	0.202	0.157	1.214	4.436
5A	0.825	1.572	0.619	−0.088	−0.185	−0.043	0.688	−0.881	0.039	0.048	1.118	4.206
5B	0.825	1.572	−0.126	0.246	−0.547	0.119	−0.157	1.269	0.052	0.067	1.278	4.206
5C	0.825	1.572	−0.297	−0.137	−0.629	−0.067	−0.339	−1.103	0.042	0.060	1.154	4.206
5D	0.825	1.572	0.525	0.375	−0.230	0.182	0.732	1.328	0.142	0.117	1.516	4.206
5E	0.825	1.572	−1.004	−0.029	−0.972	−0.014	−1.188	−0.189	0.090	0.089	1.202	4.206
5F	0.825	1.572	−0.610	0.638	−0.781	0.310	−0.970	1.717	0.522	0.500	1.972	4.206
5G	0.825	1.572	0.967	−0.147	−0.016	−0.071	1.292	−0.584	0.082	0.117	1.418	4.206
5H	0.825	1.572	0.902	0.209	−0.047	0.101	1.228	0.788	0.104	0.076	1.459	4.206
5I	0.825	1.572	0.039	−0.225	−0.466	−0.109	0.047	−1.249	0.088	0.074	1.250	4.206
5J	0.825	1.572	−0.933	0.061	−0.938	0.029	−1.077	0.453	0.070	0.082	1.168	4.206

TABLE II. (*Continued*)

Traj.	P_{lab} (GeV/c)	$E_{c.m.}$ (GeV)	Rez	Imz	Ret[a] (GeV^2)	Imt (GeV^2)	Rew[b]	Imw[b]	Re[$\pm\delta(w)$][b]		Im[$\pm\delta(w)$][b]	
6*A*	0.974	1.657	0.642	−0.054	−0.218	−0.033	0.687	−0.824	0.017	0.017	1.073	3.678
6*B*	0.974	1.657	0.019	0.095	−0.597	0.058	0.021	1.099	0.047	0.065	1.099	3.678
6*C*	0.974	1.657	−0.275	0.000	−0.776	0.000	−0.275	−0.961	0.000	0.000	1.000	3.678
6*D*	0.974	1.657	0.869	0.376	−0.080	0.229	1.301	1.133	0.395	0.274	1.725	3.678
6*E*	0.974	1.657	−1.134	−0.026	−1.298	−0.016	−1.672	−0.080	0.243	0.168	1.674	3.678
6*F*	0.974	1.657	−0.313	0.361	−0.799	0.219	−0.424	1.383	0.096	0.117	1.446	3.678
6*G*	0.974	1.657	1.020	−0.213	0.012	−0.130	1.485	−0.682	0.106	0.146	1.634	3.678
6*H*	0.974	1.657	0.604	0.276	−0.241	0.168	0.796	1.141	0.128	0.156	1.391	3.678
6*I*	0.974	1.657	−0.239	−0.610	−0.754	−0.371	−0.366	−1.763	0.165	0.152	1.801	3.678
6*J*	0.974	1.657	−1.000	0.000	−1.216	0.000	−1.000	−0.019	0.000	0.000	1.000	3.678
7*A*	1.027	1.687	0.651	−0.029	−0.228	−0.019	0.676	−0.790	0.028	0.028	1.039	3.534
7*B*	1.027	1.687	0.045	0.000	−0.623	0.000	0.045	0.999	0.000	0.000	1.000	3.534
7*C*	1.027	1.687	−0.257	0.000	−0.820	0.000	−0.257	−0.966	0.000	0.000	1.000	3.534
7*D*	1.027	1.687	1.542	0.574	0.354	0.375	2.787	1.284	2.260	2.185	3.069	3.534
7*E*	1.027	1.687	−1.004	−0.018	−1.308	−0.011	−1.152	−0.137	0.133	0.126	1.160	3.534
7*F*	1.027	1.687	−0.288	0.289	−0.841	0.189	−0.371	1.293	0.078	0.085	1.345	3.534
7*G*	1.027	1.687	1.113	−0.033	0.074	−0.022	1.608	−0.107	0.356	0.267	1.611	3.534
7*H*	1.027	1.687	0.716	0.229	−0.185	0.150	0.931	0.994	0.093	0.082	1.362	3.534
7*I*	1.027	1.687	−0.400	−0.625	−0.914	−0.408	−0.622	−1.756	0.218	0.202	1.863	3.534
7*J*	1.027	1.687	−1.089	0.066	−1.364	0.043	−1.544	0.224	0.284	0.211	1.560	3.534
8*A*	1.077	1.714	0.667	0.000	−0.232	0.000	0.667	−0.745	0.000	0.000	1.000	3.413
8*B*	1.077	1.714	0.014	0.068	−0.685	0.047	0.015	1.070	0.033	0.067	1.070	3.413
8*C*	1.077	1.714	−0.215	−0.075	−0.844	−0.052	−0.231	−1.055	0.014	0.024	1.080	3.413
8*D*	1.077	1.714	1.379	0.332	0.263	0.231	2.380	0.791	1.285	1.074	2.507	3.413
8*E*	1.077	1.714	−0.967	−0.036	−1.368	−0.025	−1.090	−0.320	0.024	0.045	1.136	3.413
8*F*	1.077	1.714	−0.335	0.161	−0.928	0.112	−0.392	1.119	0.041	0.039	1.186	3.413
8*G*	1.077	1.714	1.128	−0.113	0.089	−0.079	1.687	−0.342	0.264	0.442	1.722	3.413
8*H*	1.077	1.714	0.793	0.130	−0.144	0.090	0.953	0.773	0.037	0.037	1.227	3.413
8*I*	1.077	1.714	−0.567	−0.538	−1.089	−0.374	−0.864	−1.565	0.177	0.157	1.787	3.413
8*J*	1.077	1.714	−0.991	0.153	−1.384	0.106	−1.354	0.571	0.101	0.067	1.469	3.413
9*A*	1.171	1.764	0.671	−0.103	−0.255	−0.080	0.763	−0.857	0.022	0.022	1.147	3.218
9*B*	1.171	1.764	−0.098	0.281	−0.851	0.218	−0.124	1.315	0.100	0.111	1.321	3.218
9*C*	1.171	1.764	−0.150	−0.070	−0.892	−0.054	−0.161	−1.061	0.010	0.017	1.073	3.218
9*D*	1.171	1.764	0.974	0.699	−0.020	0.542	1.655	1.700	1.036	1.014	2.372	3.218
9*E*	1.171	1.764	−0.935	−0.030	−1.500	−0.023	−1.012	−0.396	0.030	0.026	1.086	3.218
9*F*	1.171	1.764	−0.439	0.142	−1.116	0.110	−0.507	1.054	0.081	0.074	1.169	3.218
9*G*	1.171	1.764	1.091	−0.126	0.071	−0.098	1.591	−0.402	0.220	0.285	1.641	3.218
9*H*	1.171	1.764	0.846	0.123	−0.119	0.096	1.027	0.700	0.057	0.057	1.243	3.218
9*I*	1.171	1.764	−0.651	−0.729	−1.280	−0.565	−1.070	−1.862	0.235	0.355	2.147	3.218
9*J*	1.171	1.764	−0.972	0.281	−1.529	0.218	−1.435	0.872	0.234	0.190	1.679	3.218
10*A*	1.275	1.818	0.627	−0.096	−0.323	−0.083	0.703	−0.884	0.022	0.017	1.130	3.041
10*B*	1.275	1.818	−0.107	0.206	−0.958	0.178	−0.128	1.222	0.060	0.066	1.229	3.041
10*C*	1.275	1.818	−0.104	−0.101	−0.955	−0.087	−0.114	−1.101	0.022	0.030	1.107	3.041
10*D*	1.275	1.818	0.306	0.397	−0.600	0.344	0.424	1.435	0.136	0.157	1.497	3.041
10*E*	1.275	1.818	−0.916	−0.000	−1.658	−0.000	−0.916	−0.401	0.000	0.000	1.000	3.041
10*F*	1.275	1.818	−0.633	0.066	−1.414	0.057	−0.687	0.844	0.047	0.047	1.088	3.041
10*G*	1.275	1.818	1.003	−0.006	0.003	−0.005	1.101	−0.067	0.227	0.075	1.103	3.041
10*H*	1.275	1.818	0.846	0.044	−0.133	0.038	0.915	0.583	0.082	0.057	1.085	3.041
10*I*	1.275	1.818	−0.333	−0.471	−1.153	−0.408	−0.480	−1.536	0.138	0.142	1.609	3.041
10*J*	1.275	1.818	−1.132	0.138	−1.846	0.120	−1.712	0.409	0.236	0.225	1.760	3.041

TABLE II. (*Continued*)

Traj.	P_{lab} (GeV/c)	$E_{c.m.}$ (GeV)	Rez	Imz	Ret[a] (GeV^2)	Imt (GeV^2)	Rew[b]	Imw[b]	Re[$\pm\delta(w)$][b]		Im[$\pm\delta(w)$][b]	
11*A*	1.356	1.860	0.626	−0.127	−0.350	−0.119	0.726	−0.923	0.030	0.026	1.175	2.925
11*B*	1.356	1.860	0.060	0.243	−0.880	0.228	0.074	1.271	0.084	0.097	1.273	2.925
11*C*	1.356	1.860	−0.209	−0.110	−1.132	−0.103	−0.232	−1.094	0.024	0.028	1.119	2.925
11*D*	1.356	1.860	0.278	0.687	−0.676	0.643	0.438	1.878	0.750	0.849	1.929	2.925
11*E*	1.356	1.860	−0.914	−0.023	−1.792	−0.021	−0.965	−0.432	0.040	0.028	1.057	2.925
11*F*	1.356	1.860	−0.672	0.103	−1.565	0.097	−0.764	0.857	0.035	0.032	1.148	2.925
11*G*	1.356	1.860	0.999	0.013	−0.001	0.012	1.110	0.130	0.340	0.169	1.118	2.925
11*H*	1.356	1.860	0.835	0.228	−0.154	0.213	1.123	0.889	0.209	0.271	1.432	2.925
11*I*	1.356	1.860	0.069	−0.684	−0.872	−0.640	0.107	−1.894	0.323	0.332	1.897	2.925
11*J*	1.356	1.860	−1.197	0.105	−2.056	0.098	−1.871	0.290	0.384	0.327	1.894	2.925
12*A*	1.438	1.900	0.605	−0.123	−0.398	−0.124	0.697	−0.933	0.022	0.022	1.165	2.822
12*B*	1.438	1.900	0.139	0.136	−0.869	0.137	0.157	1.136	0.028	0.047	1.147	2.822
12*C*	1.438	1.900	−0.276	−0.080	−1.286	−0.080	−0.299	−1.045	0.014	0.020	1.086	2.822
12*D*	1.438	1.900	0.308	1.333	−0.698	1.344	0.555	2.989	1.741	1.613	3.040	2.822
12*E*	1.438	1.900	−0.910	−0.028	−1.926	−0.028	−0.971	−0.448	0.028	0.020	1.070	2.822
12*F*	1.438	1.900	−0.666	0.121	−1.679	0.122	−0.771	0.884	0.024	0.024	1.173	2.822
12*G*	1.438	1.900	1.040	−0.012	0.040	−0.012	1.327	−0.056	0.122	0.066	1.328	2.822
12*H*	1.438	1.900	0.719	0.182	−0.284	0.183	0.895	0.922	0.055	0.055	1.285	2.822
12*I*	1.438	1.900	0.385	−0.912	−0.620	−0.920	0.650	−2.237	0.505	0.600	2.330	2.822
12*J*	1.438	1.900	−1.154	0.112	−2.172	0.113	−1.760	0.326	0.248	0.266	1.789	2.822
13*A*	1.505	1.933	0.574	−0.130	−0.455	−0.138	0.664	−0.963	0.026	0.022	1.170	2.747
13*B*	1.505	1.933	0.186	0.153	−0.869	0.163	0.214	1.148	0.037	0.051	1.168	2.747
13*C*	1.505	1.933	−0.282	−0.058	−1.368	−0.062	−0.299	−1.020	0.014	0.028	1.063	2.747
13*D*	1.505	1.933	−2.062	0.031	−3.268	0.033	−3.865	0.066	5.410	5.789	3.865	2.747
13*E*	1.505	1.933	−0.910	−0.058	−2.039	−0.062	−1.031	−0.493	0.035	0.024	1.143	2.747
13*F*	1.505	1.933	−0.677	0.161	−1.790	0.172	−0.819	0.928	0.039	0.046	1.238	2.747
13*G*	1.505	1.933	1.057	−0.034	0.060	−0.037	1.411	−0.137	0.210	0.165	1.418	2.747
13*H*	1.505	1.933	0.642	0.138	−0.383	0.147	0.754	0.925	0.036	0.048	1.193	2.747
13*I*	1.505	1.933	1.326	−0.457	0.348	−0.488	2.297	−1.082	1.297	1.661	2.539	2.747
13*J*	1.505	1.933	−1.144	0.229	−2.289	0.244	−1.792	0.633	0.734	0.804	1.900	2.747
14*A*	1.601	1.979	0.592	−0.157	−0.471	−0.181	0.703	−0.986	0.042	0.042	1.211	2.652
14*B*	1.601	1.979	0.278	0.117	−0.832	0.135	0.312	1.086	0.042	0.060	1.130	2.652
14*C*	1.601	1.979	−0.324	−0.047	−1.526	−0.054	−0.340	−0.994	0.014	0.032	1.050	2.652
14*D*	1.601	1.979	−0.515	0.600	−1.747	0.691	−0.800	1.684	0.419	0.420	1.864	2.652
14*E*	1.601	1.979	−0.919	−0.046	−2.212	−0.053	−1.023	−0.457	0.045	0.035	1.120	2.652
14*F*	1.601	1.979	−0.746	0.148	−2.012	0.171	−0.904	0.849	0.062	0.057	1.240	2.652
14*G*	1.601	1.979	1.002	−0.073	0.002	−0.084	1.271	−0.346	0.096	0.089	1.317	2.652
14*H*	1.601	1.979	0.654	0.100	−0.399	0.116	0.739	0.869	0.040	0.047	1.141	2.652
14*I*	1.601	1.979	0.751	−0.800	−0.287	−0.922	1.269	−1.959	0.745	0.756	2.334	2.652
14*J*	1.601	1.979	−1.146	0.008	−2.473	0.009	−1.705	0.023	0.466	0.381	1.706	2.652
15*A*	1.688	2.020	0.562	−0.144	−0.539	−0.178	0.658	−0.990	0.033	0.030	1.188	2.576
15*B*	1.688	2.020	0.330	0.218	−0.824	0.268	0.404	1.189	0.087	0.084	1.256	2.576
15*C*	1.688	2.020	−0.333	−0.000	−1.640	−0.000	−0.333	−0.943	0.000	0.000	1.000	2.576
15*D*	1.688	2.020	−0.347	0.527	−1.657	0.649	−0.515	1.616	0.228	0.279	1.696	2.576
15*E*	1.688	2.020	−0.901	−0.043	−2.339	−0.053	−0.989	−0.487	0.041	0.036	1.102	2.576
15*F*	1.688	2.020	−0.785	0.137	−2.196	0.169	−0.950	0.793	0.056	0.054	1.237	2.576
15*G*	1.688	2.020	0.944	−0.064	−0.068	−0.079	1.107	−0.437	0.062	0.047	1.190	2.576
15*H*	1.688	2.020	0.637	0.079	−0.446	0.097	0.702	0.856	0.041	0.052	1.107	2.576
15*I*	1.688	2.020	0.887	−1.248	−0.138	−1.535	1.617	−2.765	1.255	1.657	3.204	2.576
15*J*	1.688	2.020	−1.100	0.024	−2.583	0.029	−1.559	0.080	0.381	0.299	1.561	2.576

TABLE II. (*Continued*)

Traj.	P_{lab} (GeV/c)	$E_{c.m.}$ (GeV)	Rez	Imz	Ret[a] (GeV^2)	Imt (GeV^2)	Rew[b]	Imw[b]	Re[$\pm\delta(w)$][b]		Im[$\pm\delta(w)$][b]	
16*A*	1.767	2.056	0.580	−0.118	−0.547	−0.154	0.663	−0.946	0.026	0.030	1.155	2.514
16*B*	1.767	2.056	0.332	0.255	−0.869	0.332	0.418	1.237	0.097	0.104	1.305	2.514
16*C*	1.767	2.056	−0.341	−0.051	−1.744	−0.066	−0.359	−0.992	0.014	0.028	1.055	2.514
16*D*	1.767	2.056	−0.457	0.405	−1.896	0.527	−0.643	1.400	0.200	0.178	1.540	2.514
16*E*	1.767	2.056	−0.917	−0.055	−2.493	−0.071	−1.036	−0.476	0.066	0.048	1.140	2.514
16*F*	1.767	2.056	−0.855	0.141	−2.412	0.183	−1.063	0.718	0.107	0.114	1.283	2.514
16*G*	1.767	2.056	0.957	−0.062	−0.056	−0.081	1.129	−0.407	0.071	0.060	1.200	2.514
16*H*	1.767	2.056	0.627	0.080	−0.486	0.104	0.691	0.866	0.044	0.046	1.108	2.514
16*I*	1.767	2.056	1.232	−1.295	0.302	−1.684	2.290	−2.803	2.152	2.228	3.620	2.514
16*J*	1.767	2.056	−1.136	0.012	−2.778	0.016	−1.674	0.037	0.750	0.507	1.674	2.514
17*A*	1.872	2.103	0.557	−0.118	−0.618	−0.164	0.635	−0.960	0.032	0.028	1.151	2.440
17*B*	1.872	2.103	0.167	0.169	−1.163	0.236	0.195	1.170	0.040	0.045	1.186	2.440
17*C*	1.872	2.103	−0.330	−0.070	−1.856	−0.098	−0.355	−1.017	0.017	0.026	1.077	2.440
17*D*	1.872	2.103	−0.525	0.249	−2.127	0.347	−0.670	1.147	0.062	0.069	1.328	2.440
17*E*	1.872	2.103	−0.807	−0.166	−2.521	−0.232	−1.013	−0.814	0.083	0.062	1.300	2.440
17*F*	1.872	2.103	−0.841	0.105	−2.568	0.146	−0.995	0.677	0.044	0.054	1.203	2.440
17*G*	1.872	2.103	0.971	−0.076	−0.041	−0.107	1.192	−0.412	0.131	0.145	1.261	2.440
17*H*	1.872	2.103	0.645	0.034	−0.496	0.047	0.673	0.800	0.039	0.039	1.045	2.440
17*I*	1.872	2.103	1.207	−0.198	0.288	−0.277	1.931	−0.529	0.696	0.600	2.002	2.440
17*J*	1.872	2.103	−0.988	−0.022	−2.774	−0.030	−1.100	−0.213	0.147	0.118	1.120	2.440
18*A*	1.975	2.148	0.518	−0.181	−0.718	−0.269	0.624	−1.062	0.051	0.049	1.232	2.376
18*B*	1.975	2.148	0.250	0.363	−1.117	0.540	0.337	1.401	0.194	0.179	1.441	2.376
18*C*	1.975	2.148	−0.339	−0.023	−1.993	−0.035	−0.348	−0.964	0.024	0.055	1.025	2.376
18*D*	1.975	2.148	−0.283	0.387	−1.909	0.576	−0.388	1.427	0.176	0.163	1.478	2.376
18*E*	1.975	2.148	−0.804	−0.091	−2.685	−0.135	−0.924	−0.704	0.032	0.028	1.161	2.376
18*F*	1.975	2.148	−0.747	0.120	−2.599	0.178	−0.877	0.808	0.044	0.039	1.192	2.376
18*G*	1.975	2.148	0.856	−0.158	−0.214	−0.235	1.086	−0.745	0.088	1.317	1.317	2.376
18*H*	1.975	2.148	0.656	0.115	−0.512	0.171	0.753	0.885	0.050	0.050	1.162	2.376
18*I*	1.975	2.148	1.258	−0.049	0.383	−0.073	2.032	−0.130	0.655	0.478	2.027	2.376
18*J*	1.975	2.148	−1.000	−0.000	−2.976	−0.000	−1.000	0.024	0.000	0.000	1.000	2.376
19*A*	2.055	2.183	0.523	−0.082	−0.744	−0.128	0.573	−0.940	0.032	0.042	1.101	2.331
19*B*	2.055	2.183	0.159	0.284	−1.312	0.443	0.204	1.312	0.133	0.132	1.328	2.331
19*C*	2.055	2.183	−0.319	−0.000	−2.058	−0.000	−0.319	−0.948	0.000	0.000	1.000	2.331
19*D*	2.055	2.183	−0.293	0.416	−2.018	0.650	−0.410	1.466	0.314	0.214	1.522	2.331
19*E*	2.055	2.183	−0.785	−0.039	−2.786	−0.061	−0.835	−0.661	0.042	0.047	1.065	2.331
19*F*	2.055	2.183	−0.741	0.087	−2.717	0.136	−0.835	0.771	0.047	0.045	1.136	2.331
19*G*	2.055	2.183	0.878	−0.091	−0.190	−0.141	1.034	−0.601	0.057	0.056	1.196	2.331
19*H*	2.055	2.183	0.719	0.097	−0.438	0.151	0.818	0.805	0.037	0.042	1.148	2.331
19*I*	2.055	2.183	1.973	0.077	1.518	0.120	3.674	0.166	2.369	2.030	3.678	2.331
19*J*	2.055	2.183	−1.010	0.001	−3.137	0.002	−1.155	0.011	0.157	0.079	1.155	2.331
20*A*	2.267	2.260	0.504	−0.171	−0.879	−0.303	0.602	−1.057	0.109	0.141	1.216	2.218
20*B*	2.267	2.260	−0.008	0.246	−1.786	0.436	−0.010	1.276	0.162	0.165	1.276	2.218
20*C*	2.267	2.260	−0.301	−0.074	−2.306	−0.132	−0.325	−1.031	0.026	0.026	1.081	2.218
20*D*	2.267	2.260	−0.276	0.436	−2.261	0.773	−0.389	1.498	0.489	0.365	1.547	2.218
20*E*	2.267	2.260	−0.772	−0.100	−3.140	−0.177	−0.890	−0.754	0.044	0.044	1.166	2.218
20*F*	2.267	2.260	−0.742	0.000	−3.087	0.000	−0.742	0.670	0.000	0.000	1.000	2.218
20*G*	2.267	2.260	0.733	−0.038	−0.474	−0.068	0.774	−0.721	0.094	0.118	1.058	2.218
20*H*	2.267	2.260	0.707	0.208	−0.520	0.368	0.899	0.970	0.121	0.081	1.322	2.218
20*I*	2.267	2.260	1.053	0.092	0.094	0.162	1.452	0.334	0.170	0.151	1.490	2.218
20*J*	2.267	2.260	−1.006	−0.005	−3.554	−0.010	−1.122	−0.053	0.153	0.076	1.123	2.218

[a] See Fig. 8 for plots of (Ret vs $E_{c.m.}$).

[b] See Figs. 7 for plots in w plane. (Errors on the critical point positions have been artificially set to zero for commodity. See Ref. 15 for details.)

[c] See Fig. 10 for the plot of the distance w_r to the physical region in the w plane vs P_{lab}. (These distances have been calculated before the resolution of the discrete ambiguity, assuming all trajectories in the w plane are outside the unit circle. Solutions inside would have Im(z) and Im(t) changed sign, w replaced by conj(1/w), w_r and R_w replaced by their inverse.)

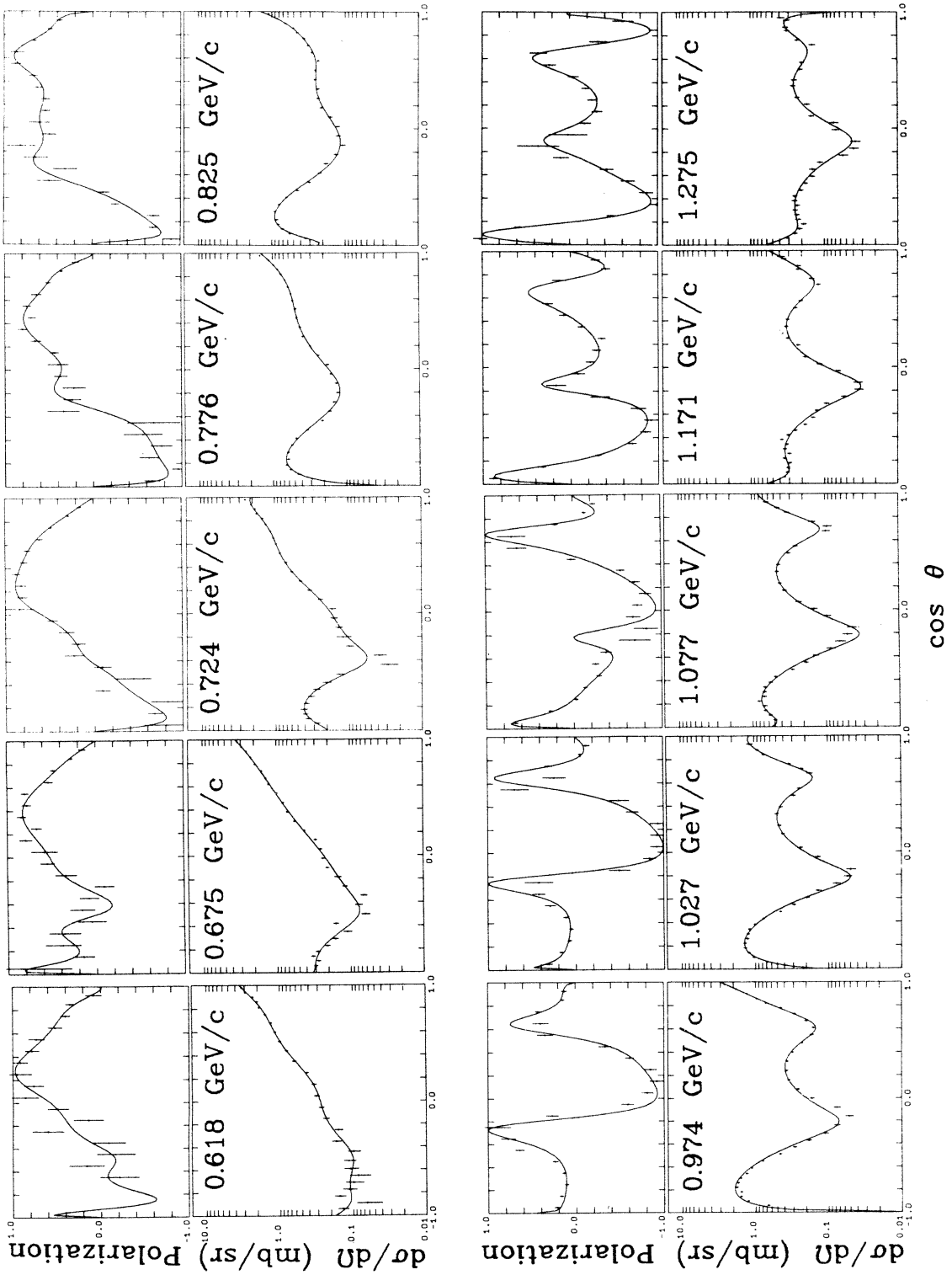

FIG. 6. B76 data and $N=10$ polynomial representation thereof.

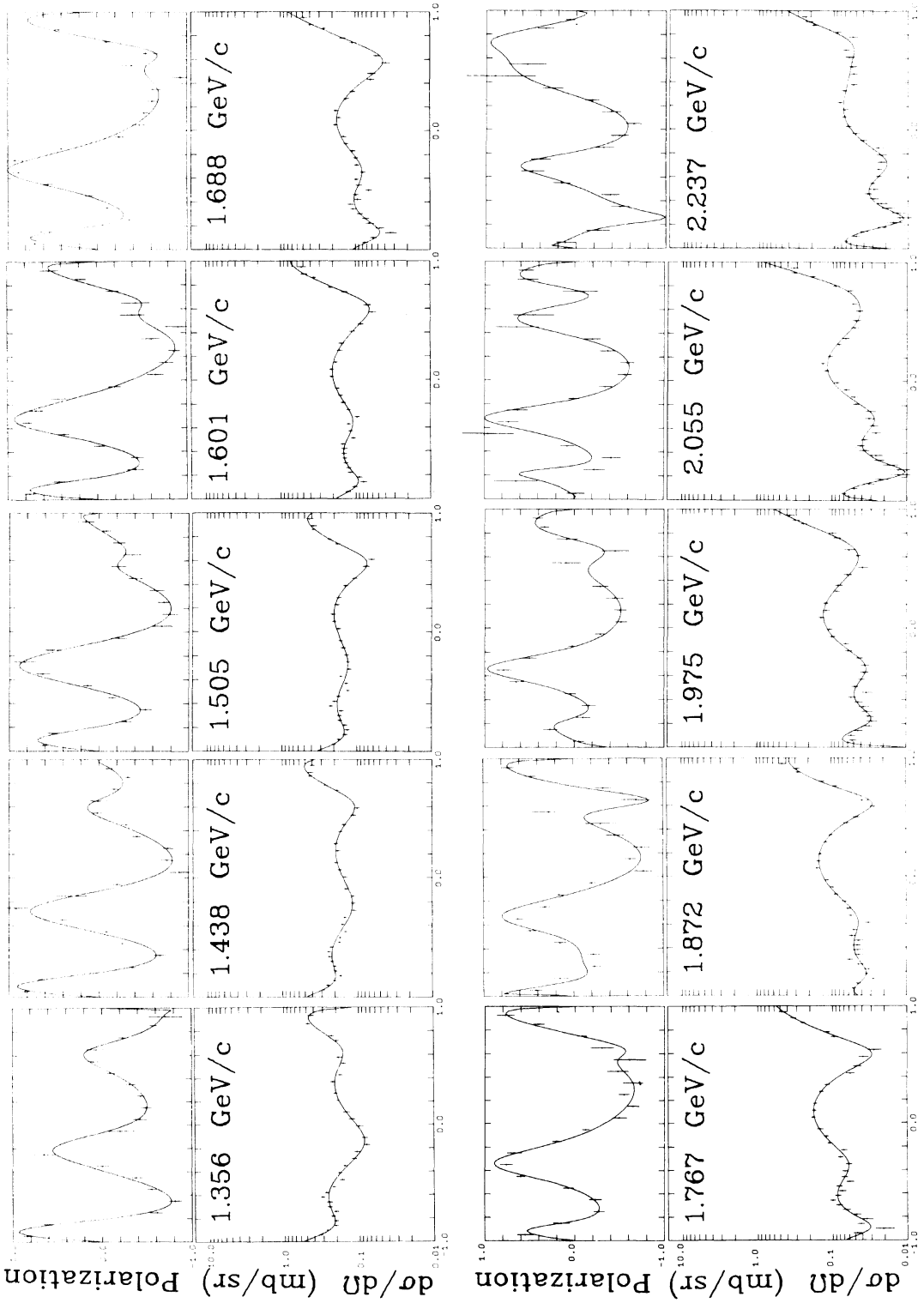

FIG. 6. *(continued)*

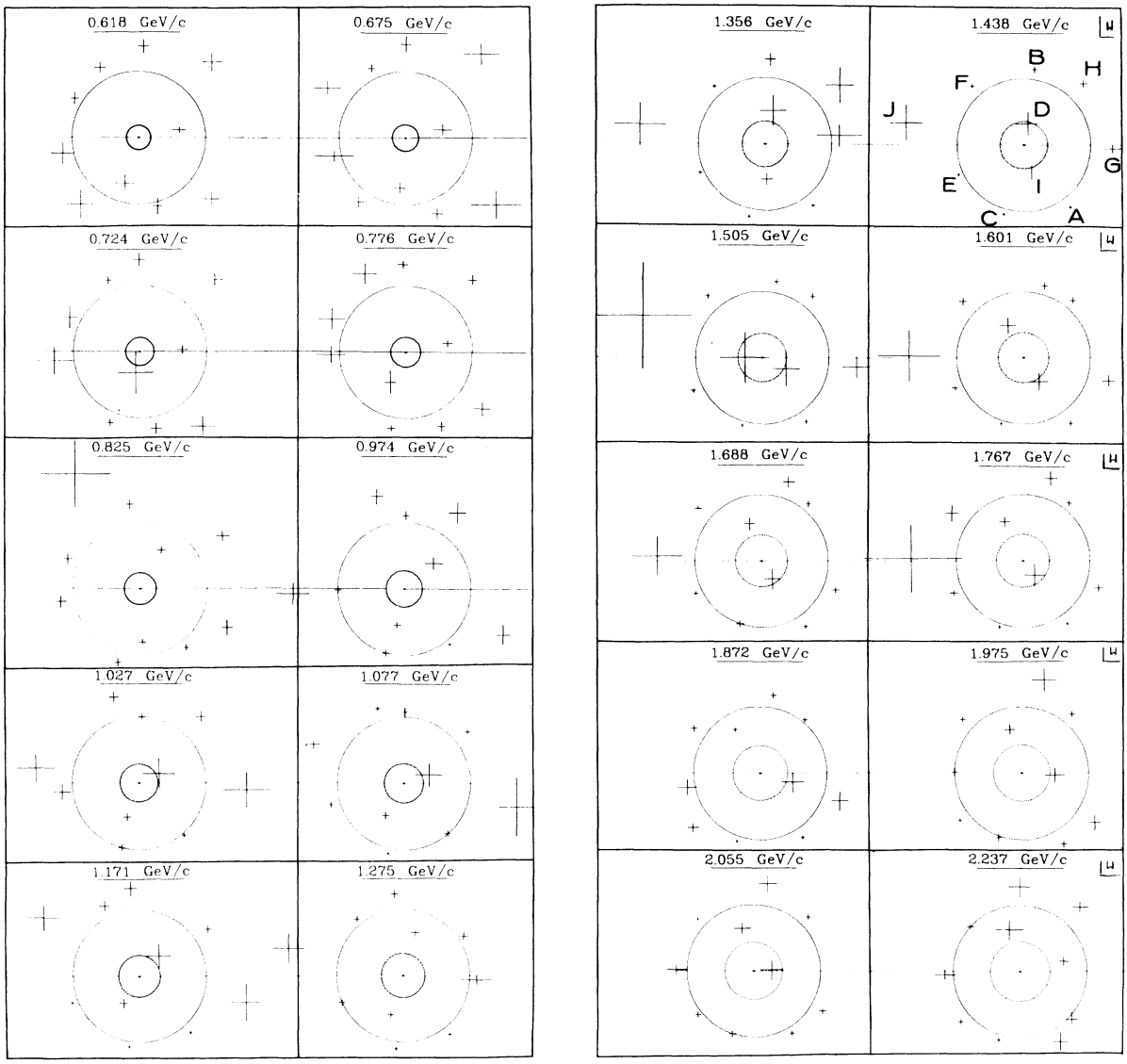

FIG. 7. Location of the zeros of the 10th-order polynomial fit in the w plane for the 20 energies of the B76 data.

with four stars. If the error bar does not overlap $P = \pm 1$ (or if there are no data at the $\cos\theta$ value where the polynomial representation of P reaches ± 1), we list the critical point with two stars.

Two considerations leave open the door to additional critical points: (1) The possibility of systematic error in polarization normalization. That is, even though the measured polarization or the polynomial representation thereof fail to reach ± 1, both might do so if $|P|$ were enlarged by, say 10%. To explore this possibility we have allowed 10% variation in the normalization of the B76 polarization data and repeated our analysis. Critical points thereby found are assigned three stars. When found close to ("coincident" with) a four- or two-star candidate we regard the critical point to be confirmed.[24] (2) There is also the possibility that a critical point occurs at an energy between two adjacent measured energies, with such rapid change of polarization that at neither of the measured energies is P compatible with ± 1. It is in fact typically the case that the rate of change of P is unusually high near a critical point. So where we observe a rapid energy variation of P near a polarization extremum we list a one-star possible critical point in Table III. Such critical points evidently have a lower confidence level, but when found in coincidence with

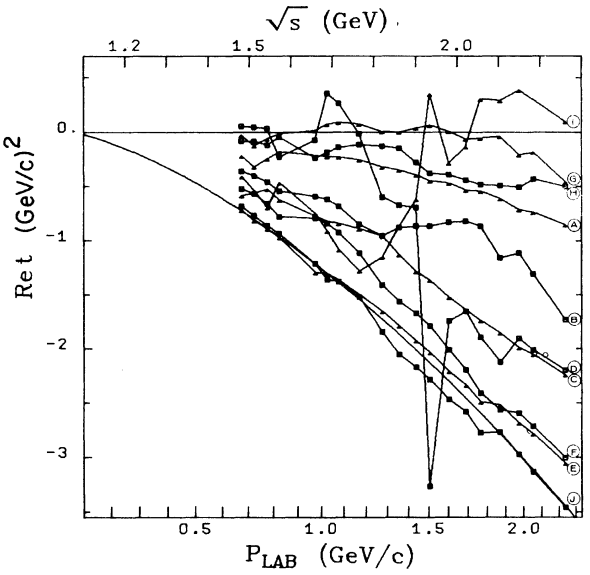

FIG. 8. Ret versus $\sqrt{s}$ and p_{1ab}.

three-star critical points we consider them "confirmed".[25]

VII. RESOLUTION OF THE DISCRETE AMBIGUITY

Given the critical points it remains to establish for each trajectory at some particular energy whether it lies inside or outside the unit circle. The discrete ambiguity will thereby be removed at all energies. We here invoke the assumption that there exist individual reasonably sharp resonances of well-defined angular momentum J and naturality ϵ, so that near such a resonance the stable zeros are fairly close in position to the $2J-1$ zeros of the polynomial $R_{J,\epsilon}(w)$ which are either all inside ($\epsilon=+1$) or all outside ($\epsilon=-1$) the unit circle. As the resonance is approached, the "extra" zeros should become unstable. (According to causality considerations, the $2J-1$ surviving zeros should move in a clockwise sense about the positions of the zeros of $R_{J,\epsilon}(w)$.

In the neighborhood of the strong $\frac{7}{2}^+$ resonance near 1900 MeV ($P_{1ab}\sim 1.5$ GeV/c) one does indeed observe (in Fig. 10) that six zeros (three each in Σ^+ and Σ^-) are close to the physical region while four (two each in Σ^+ and Σ^-) are substantially further away. Since the zeros of $R_{7/2,+}(w)$ all lie inside the unit circle, it is reasonable to assume at this energy that the six nearest Barrelet zeros also lie inside. What about the remaining four? The next resonance in the same Regge sequence is $\frac{11}{2}^+$ at 2420 MeV ($P_{1ab}\sim 2.6$ GeV/c). It is then plausible that all ten of our trajectories should at that point lie inside the unit circle, close to the physical region. Inspection of Fig. 7 or 10 shows that above $P_{1ab}=2.2$ GeV/c all ten zeros are indeed well inside the strip of convergence. A knowledge of critical points between $P_{1ab}=2.2$ and $P_{1ab}=2.6$ GeV/c would resolve the discrete ambiguity for all ten trajectories. Lacking such information we still can anchor six of the trajectories to the $\frac{7}{2}^+$ resonance.

The presence of critical points in all four of the nearby zeros near $P_{1ab}=1.0$ GeV/c (A, B, C, and F) and the general instability here of the remaining zeros is attributed to the proximity of both $\frac{5}{2}^+$ and $\frac{5}{2}^-$ resonances. The four zeros of $R_{5/2,+}$ lie inside the unit circle while those of $R_{5/2,-}$ lie outside.[26]

Combining our critical points with the $\frac{7}{2}^+$ anchor, we are able to resolve the discrete ambiguity for the six trajectories (A, H, C, B, E, and F) of Table II, the positions of the zeros heretofore given outside are modified according to the results given in Table III and Fig. 10 (where the part of the trajectories inside the unit circle has been dotted). The uncertainties in this resolution of the discrete ambiguity come mainly from the nonconfirmed one-star critical points: The results could change drastically for B (below 1.438 and/or above 1.688 GeV/c) and E (above 2.055).

We have tentatively resolved the remaining discrete ambiguity by making the following guesses for the interval between 2.3 and 2.4 GeV about the four trajectories G, I, D, J that are far from the physical region near the $\Delta\frac{7}{2}^+$ resonance around 1.9 GeV: (a) Trajectories G and I, which seem to be heading for the physical region at 2.3 GeV each have one critical point before 2.4 GeV.[27] Trajectory D, which is still far away at 2.3 GeV, has no critical point before 2.4 GeV (and is therefore assigned the inside location throughout the whole energy range that we have studied). (c) Trajectory I, which has a critical point near 2.3 GeV, has no further critical point before 2.4 GeV. If subsequent experiments indicate otherwise, it will be easy to modify the results.

The zeros under discussion are zeros of the amplitude $F(w)$, which is related to the measured quantity $\Sigma(w)$ by

$$\Sigma(w)=F(w)\overline{F}(\overline{w}^{-1}).$$

Consequently, once the positions of nearby zeros in the complex w plane are established, one can place heavy constraints on partial-wave analysis and, with information about the modulus and phase at one angle (such as $\theta=0$) can even make an approximate construction of the amplitude.[5] We defer the latter attempt to a subsequent paper.

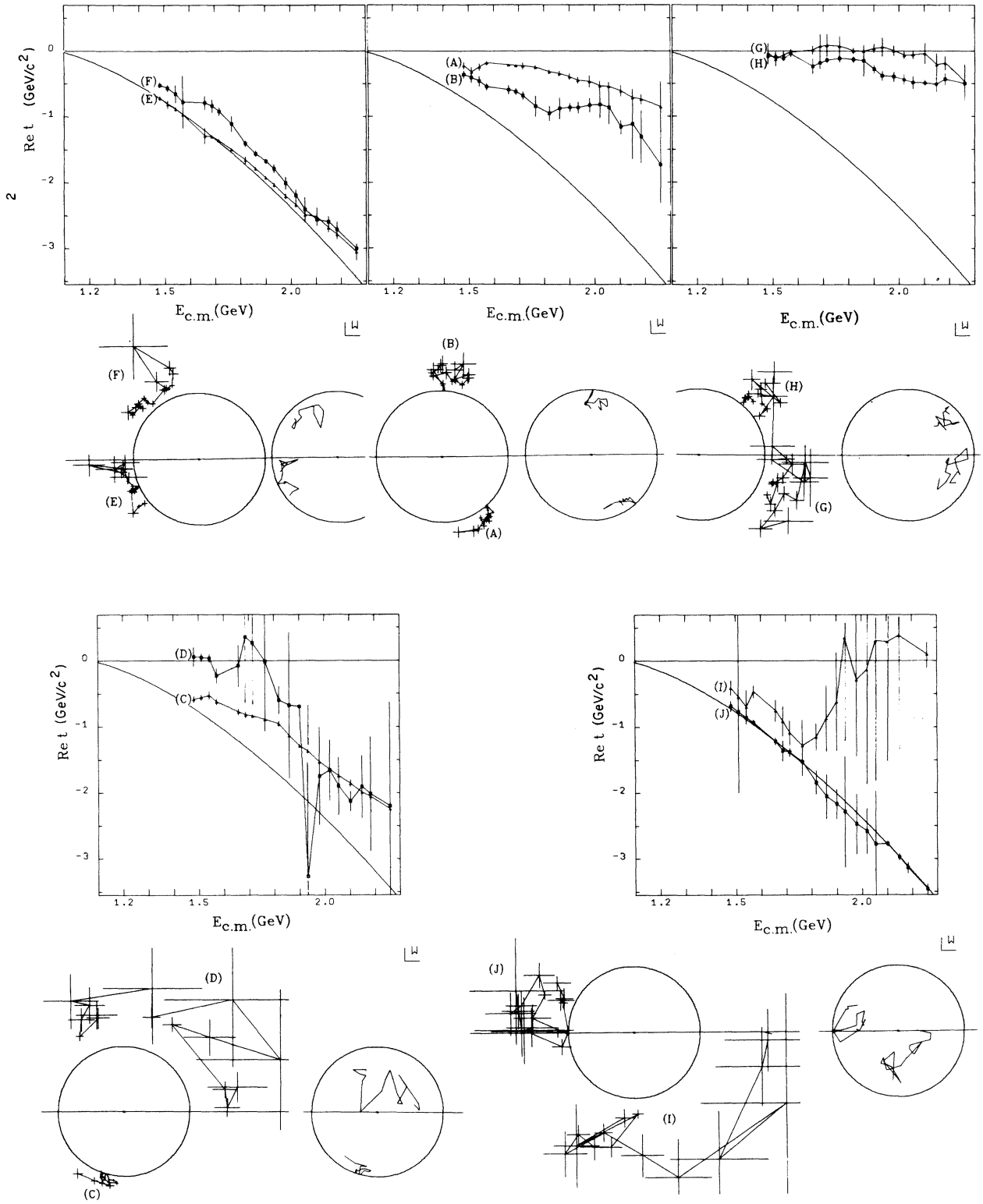

FIG. 9. Detail of Fig. 8 with errors and corresponding location of the trajectories in the w plane, either outside (with errors on the zero position) or inside the unit circle.

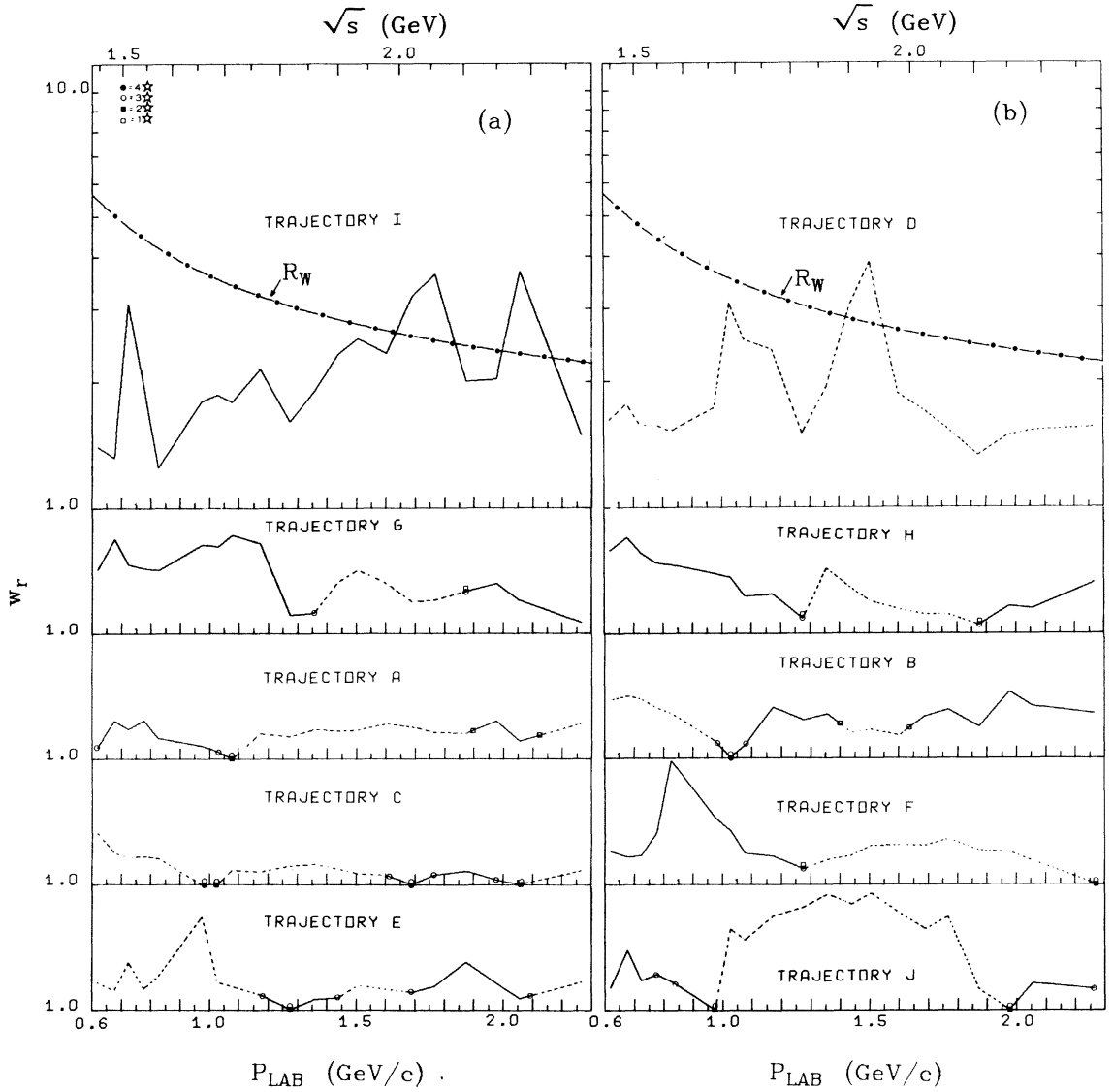

FIG. 10. $w_r \equiv |w|$ versus p_{lab}, assuming all zeros outside, for the trajectories of (a) Σ^- (corresponding to maxima of the polarization), and (b) Σ^+ (corresponding to minima of the polarization). Critical points are indicated according to their level of confidence increasing from one star (□), two stars (■), three stars (○), and four stars (●). The part of the trajectory which is found inside the unit circle after the resolution of the discrete ambiguity has been dotted. The curve above represents the outside boundary of the disk of convergence of the polynomial expansion, assuming the first singularity to be the ρ.

VIII. CONCLUSION

We have shown how Barrelet-moment analysis can reveal systematic errors in $\pi^- p$ charge-exchange data. Selecting data which does not show symptoms of important systematic error, we have then determined the nearby zeros of the polarized cross section $\Sigma(w)$. The energy interval covered by this data is 1.45 GeV $< \sqrt{s} <$ 2.3 GeV. Within this interval ten nearby zeros are found, and we give arguments to resolve the discrete ambiguity that arises for the position of each when it is regarded as a zero in the amplitude.

Our analysis depends heavily on identification of critical points and calls attention to the importance of more accurate experiments at those energies where we suggest that critical points occur. Our argument for resolving the discrete ambiguity for all ten zeros underlines the usefulness of extending the measured energy range all the way up to the $\Delta \frac{11}{2}^+$ resonance.

TABLE III. Critical points and resolution of the discrete ambiguity.

P_{lab} (GeV/c)	Critical points[a] 4*	3*	2*	1*	Discrete ambiguity A	B	C	D	E	F	G	H	I	J
					I	I	I	I	I	O	O	O	O	O
0.618		A			O	I	I	I	I	O	O	O	O	O
0.675					O	I	I	I	I	O	O	O	O	O
0.724					O	I	I	I	I	O	O	O	O	O
0.776		J			O	I	I	I	I	O	O	O	O	O/I
0.825		J			O	I	I	I	I	O	O	O	O	O/I
0.974	C	B,C,J	J		O	I/O	I/O	I	I	O	O	O	O	I
1.027	B	A,B,C	C		O/I	I/O	O/I	I	I	O	O	O	O	I
1.077		A,B	A		I	O	I	I	I	O	O	O	O	I
1.170		E			I	O	I	I	I/O	O	O	O	O	I
1.275	E	E,F,H												
				F,H	I	O	I	I	O	O/I	O	O/I	O	I

P_{lab} (GeV/c)	Critical points[a] 4*	3*	2*	1*	Discrete ambiguity[b] A	B	C	D	E	F	G	H	I	J
				F,H	I	O	I	I	O	O/I	O	O	I	I
1.356		G			I	O	I	I	O	I	I	I	O	I
1.438		E		B	I	O/I	I	I	I	I	I	I	O	I
1.505					I	I	I	I	I	I	I	I	O	I
1.601		C			I	I	I/O	I	I	I	I	I	O	I
1.688	C	C,E		B,E	I	I/O	I/O	I	I/O	I	I	I	O	I
1.767		C			I	O	O	I	O	I	I	I	O	I
1.872		G,H		A,G,H	I/O	O	O	I	O	I	O	I/O	O	I
1.975		C,J	J		O	O	O/I	I	O	I	O	O	O	O
2.055		C	C	A,E	O/I	O	I	I	O/I	I	O	O	O	O
2.267		F,J	F		I	O	I	I	I	O	O	O	O	I

[a] 4*: Data and polynomial approximation show that $|P| = 1$.
3*: Data have been renormalized (by 10%) for data and polynomial approximation to show $|P| = 1$.
2*: Data are missing at the $\cos\theta$ value where the polynomial approximation shows that $|P| = 1$.
1*: Data are missing at the P_{lab} value (within 2 of the B76 P_{lab} values) where we believe a critical point would be observed.

[b] The trajectories are named after their location at $P_{lab} = 1.438$ GeV/c (see Fig. 7) and are found either inside (I) or outside (O) of the unit circle in the w plane.

ACKNOWLEDGMENTS

We are very grateful to G. F. Chew for numerous enlightening discussions and his attention to this paper. We thank R. Ely and G. Gidal for their constant encouragement and support. We also wish to acknowledge assistance by R. Kelly, of the Particle Data Group, in providing us with the data necessary for this study. This work was supported in part by the U. S. Energy Research and Development Administration under Contract No. W-7405-ENG-48.

---

*On leave from the University of Paris VI, Paris, France.

[1]Scattering data for the reaction $\pi^- p \to \pi^0 n$: The data listed below have been selected on the ground that they present more than 20 data points per energy. B64: A. Bigi *et al.*, Nuovo Cimento 34, 878 (1964); B76: R. M. Brown *et al.*, Rutherford Laboratory Report No. R1-76093, 1976 (unpublished); Nucl. Phys. B117, 12 (1976); C67: C. B. Chiu *et al.*, Phys. Rev. 156, 1415 (1967); C69: A. S. Carroll *et al.*, *ibid.* 177, 2047 (1969); N72: J. E. Nelson Ph.D. thesis, Report No. LBL-1019, 1972 (unpublished); N73: J. E. Nelson *et al.*, Phys. Lett. 47B, 281 (1973). For a complete survey of all available data, see K. H. Augemstein, G. Höhler, E. Pietarinen, and H. M. Staudenmaier, Karlsruhe Physics Data Report No. 1-2, 1977 (unpublished).

[2]Polarization data for the reaction $\pi^- p \to \pi^0 n$: B76: R. M. Brown *et al.*, Rutherford Laboratory Report No. R1-76093, 1976 (unpublished); S74: S. R. Shannon, Ph.D. thesis, LBL Report No. LBL-2607, 1974 (unpublished); S. R. Shannon *et al.*, Phys. Rev. Lett. 33, 237 (1974).

[3](a) R. Ayed and P. Bareye (Saclay), Conference on Elementary Particles, Aix-en Provence, 1973 (unpublished); and private communication to the Particle Data Group. (b) R. E. Cutkosky *et al.*, Phys. Rev. Lett. 37, 645 (1976).

[4](a) See B76 and S74 of Refs. 1 and 2. (b) R. Kelly (private communication); G. Höhler (Karlsruhe) private communication.

[5]D. M. Chew and M. Urban, LBL Report No. LBL-4656, 1976 (unpublished); in *Proceedings of the Topical Conference on Baryon Resonances, Oxford*, edited by R. T. Ross and D. H. Saxon (Rutherford Laboratory, Chilton, Didcot, England, 1977), p. 156.

[6]D. M. Chew, E. Barrelet, and M. Urban, LBL Report No. LBL-4644 (under revision and completion with more recent data) (unpublished); for preliminary results see Ref. 5.

[7]E. Barrelet, thesis, 1970 Paris (unpublished); Nuovo Cimento 8A, 331 (1972).

[8]D. M. Chew, LBL Report No. LBL-6102, 1977 (unpublished).

[9]For reasons to be explained we analyze only experiments with data from at least 20 different angles at a given energy.

[10]It is assumed that the statistical errors on all points in a given distribution are of comparable magnitude.

[11]If R is the radius of the ellipse (in the $z = \cos\theta$ plane) passing through the first singularity, then the coefficients A_l have an asymptotic behavior like $(1/R)^l$ as $l \to \infty$.

[12]D. M. Chew, LBL Report No. LBL-6406, 1977 (unpublished).

[13]The last point constitutes an important advantage over a least-square-fit method which has no way of distinguishing between correctly measured points and those affected by systematic errors.

[14]E. Barrelet and M. G. Fouque, Program Moulin, Ecole Polytechnique, 1969 (unpublished), completed for the errors by the information from Ref. 15.

[15]M. Urban, thesis, 1973 Paris (unpublished); see also LBL Report No. LBL-4809, 1976.

[16]The two highest energies could be considered from a statistical point of view but would have to be disregarded because of our finding systematic errors larger than the statistical errors.

[17]G. Höhler, H. P. Jakob, and F. Kaiser, University of Karlsruhe Report No. 7616, 1976 (unpublished).

[18]Backward-scattering data of the reaction $\pi^- p \to \pi^0 n$: A68: V. D. Antopolsky *et al.*, Phys. Lett. 28B, 223 (1968); D75: N. C. Debenham *et al.*, Phys. Rev. D 12, 2545 (1975); K72: V. Kistiakowsky *et al.*, *ibid.* 6, 1882 (1972).

[19]R. Kelly (Particle Data Group, LBL), private communication.

[20]At least for the energies of B76 which do not manifest large systematic errors.

[21]However, they may "jump" (i.e., move very rapidly away from the physical region) in an energy region dominated by a sharp resonance (see Sec. VII).

[22]Should the zeros drawn inside the unit circle be positioned outside, the error bars would be enlarged by a factor $|w|^{-2}$ (see Ref. 15).

[23]The radius of the outside boundary is the inverse of the radius of the inside boundary.

[24]A natural assumption, when the analysis yields two or more critical points at nearby energies for the same trajectory, is that there is but a single crossing of the physical region. However, near 1 GeV/c for the C trajectory there is an indication from the evidence on two-, three-, and four-star critical points that two separate crossings may occur with a spacing of ~ 50 MeV/c.

[25]The only nonconfirmed one-star critical points (by any two, three, or four star) are A (1.872–1.975 and 2.055–2.267 GeV/c), B (1.438–1.505 and 1.688–1.767 GeV/c), and E (2.055–2.267 GeV/c).

[26]These critical points explain the difficulty in the measurements of the data around 1.0 GeV/c, because, as observed in the elastic $\pi^+ p$ data (See Refs. 5 and 6), the differential cross section has the deepest minima when $P = \pm 1$. (See Fig. 6 at $P_{\text{lab}} = 1.027$ and 1.077 GeV/c).

[27]The same hypothesis has to be made for trajectories B, F and, H (unless the one-star critical point for B around 1.688 GeV/c can be experimentally cancelled)—even though for none of these trajectories are any signs of these (future) critical points apparent yet at 2.267 GeV/c within the available data.

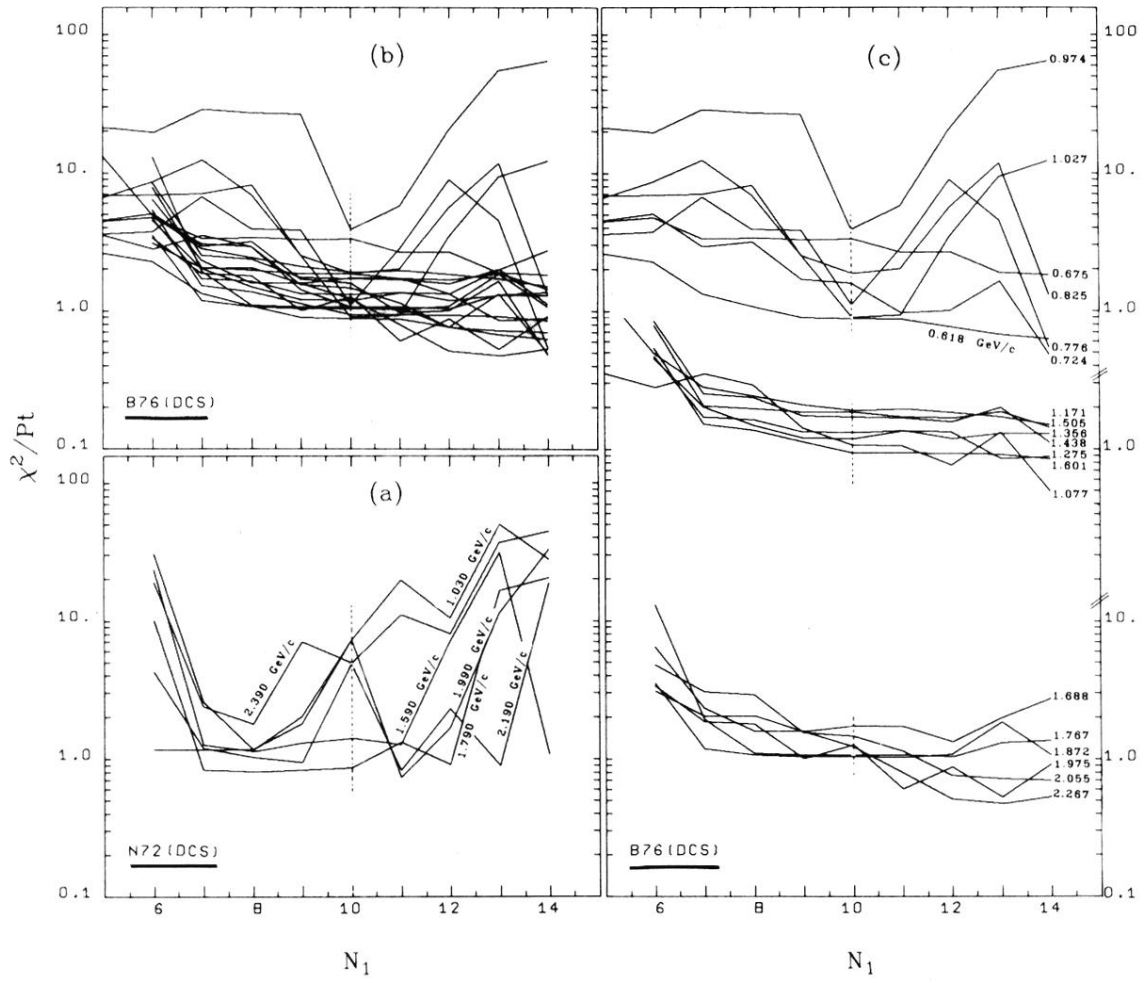

FIG. 1. χ^2 per data point vs the polynomial order N_1 for the scattering data N72 (a) and B76 (b), detailed in (c).

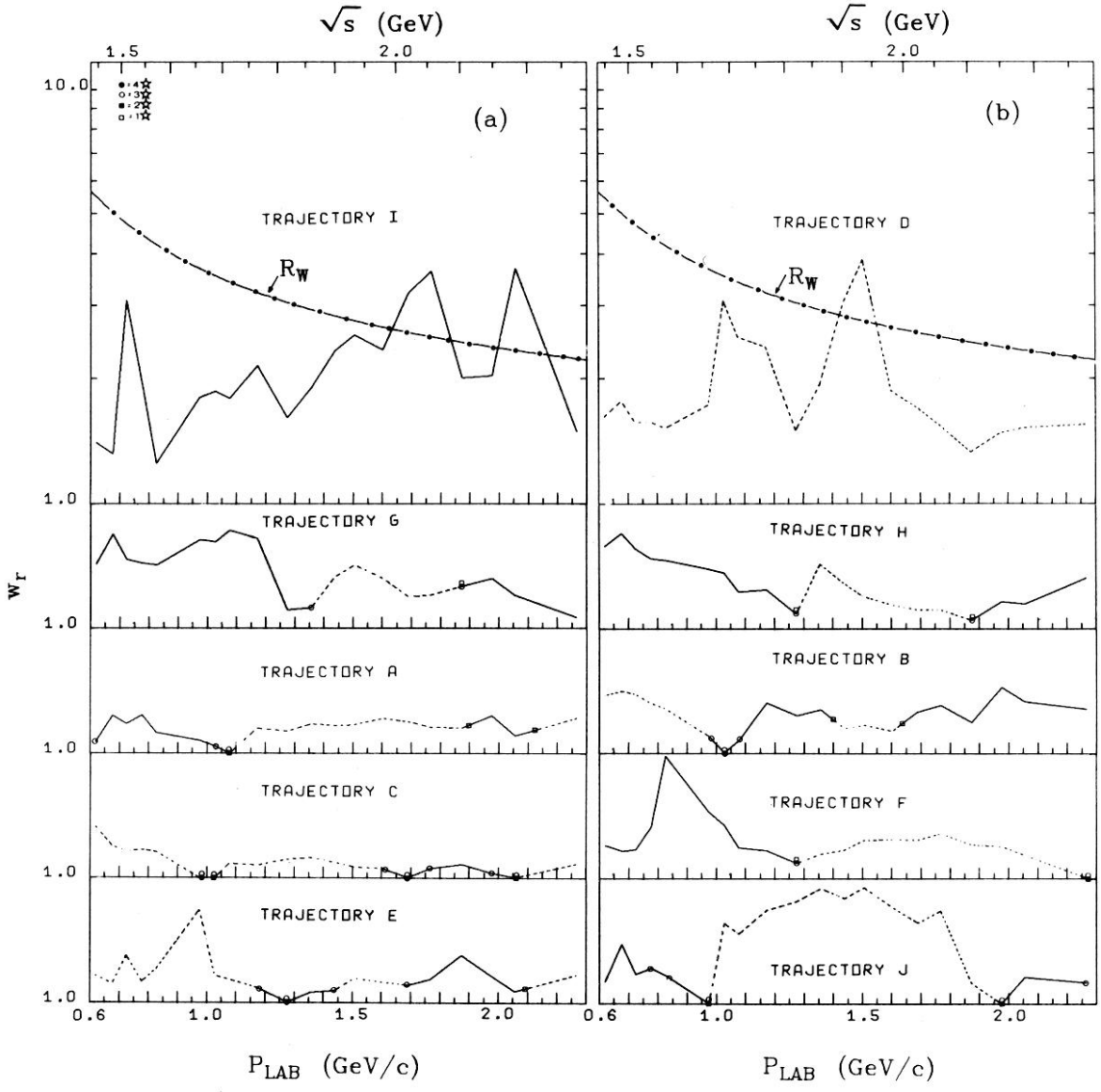

FIG. 10. $w_r \equiv |w|$ versus p_{lab}, assuming all zeros outside, for the trajectories of (a) Σ^- (corresponding to maxima of the polarization), and (b) Σ^+ (corresponding to minima of the polarization). Critical points are indicated according to their level of confidence increasing from one star (□), two stars (■), three stars (○), and four stars (●). The part of the trajectory which is found inside the unit circle after the resolution of the discrete ambiguity has been dotted. The curve above represents the outside boundary of the disk of convergence of the polynomial expansion, assuming the first singularity to be the ρ.

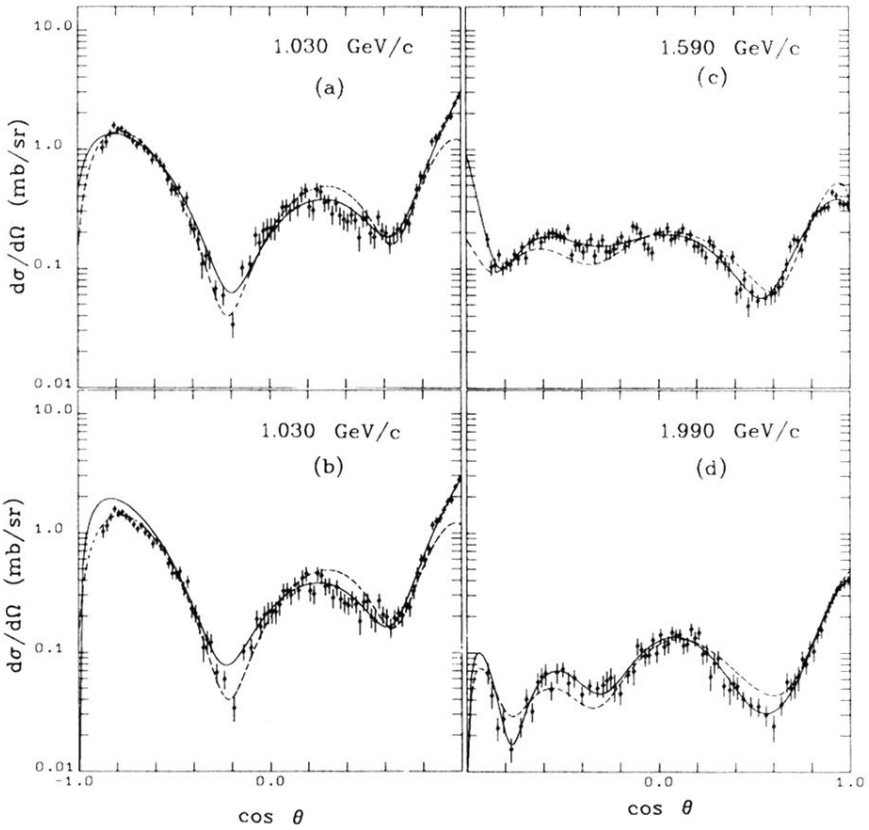

FIG. 2. Comparison of the polynomial representation of the B76 scattering data ($N_1 = 10$, dotted line) with N72 data and polynomial representation thereof [(a) $N_1 = 6$ and (b), (c), (d) $N_1 = 10$, solid line] at three closely matched energies. (The data of B76 are in Fig. 6.)

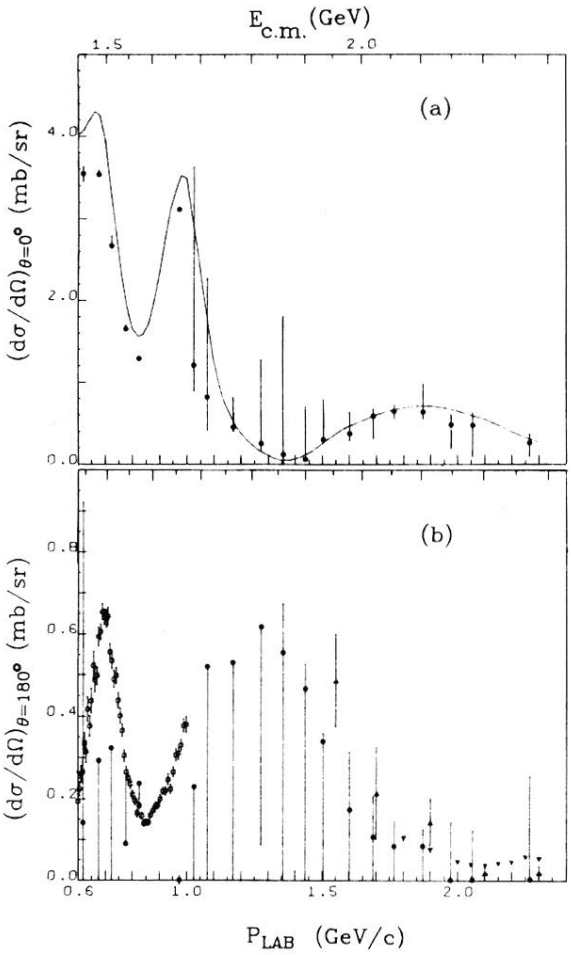

FIG. 3. (a) $(d\sigma/d\Omega)_{\theta=0}$ from extrapolation of the polynomial representation of B76 scattering data. The line is the value calculated in Ref. 17. (b) $(d\sigma/d\Omega)_{\theta=180}$ for extrapolation of the polynomial representation of B76 scattering data, compared with the data of Ref. 18, (□) for D75, (△) for A69, and (▽) for K72.

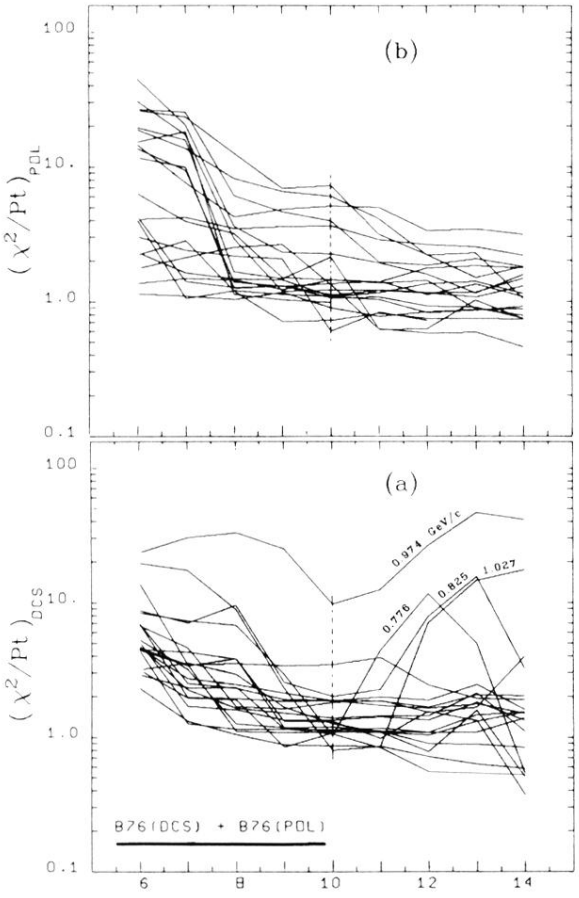

FIG. 4. χ^2 per data point versus polynomial order N when B76 scattering and polarization data are simultaneously analyzed. (a) for $d\sigma/d\Omega$, (b) for P.

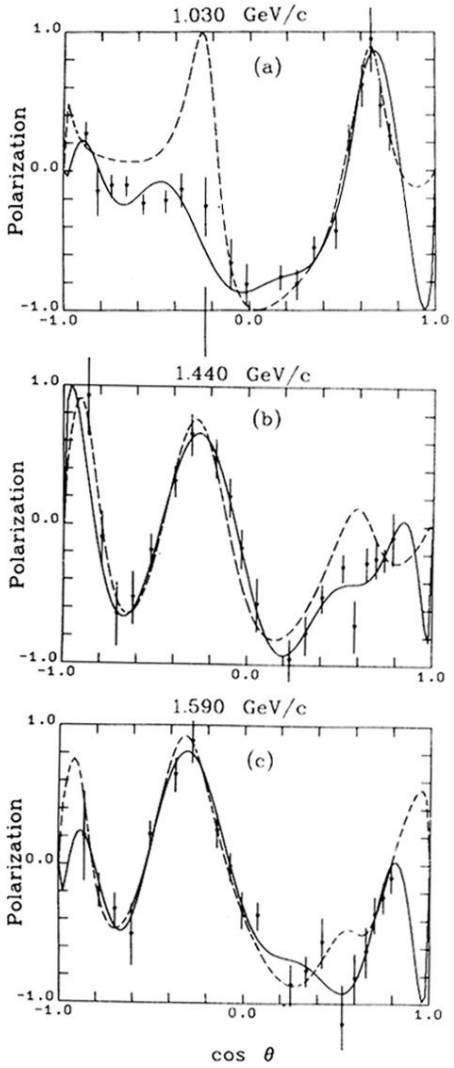

FIG. 5. Comparison of $N=10$ polynomial representation for P with S74 data at three closely matched energies, (a) 1.030 (S74) and 1.027 (B76), (b) 1.440 (S74) and 1.437 (B76), (c) 1.590 (S74) and 1.601 (B76). (The data of B76 is in Fig. 6.)

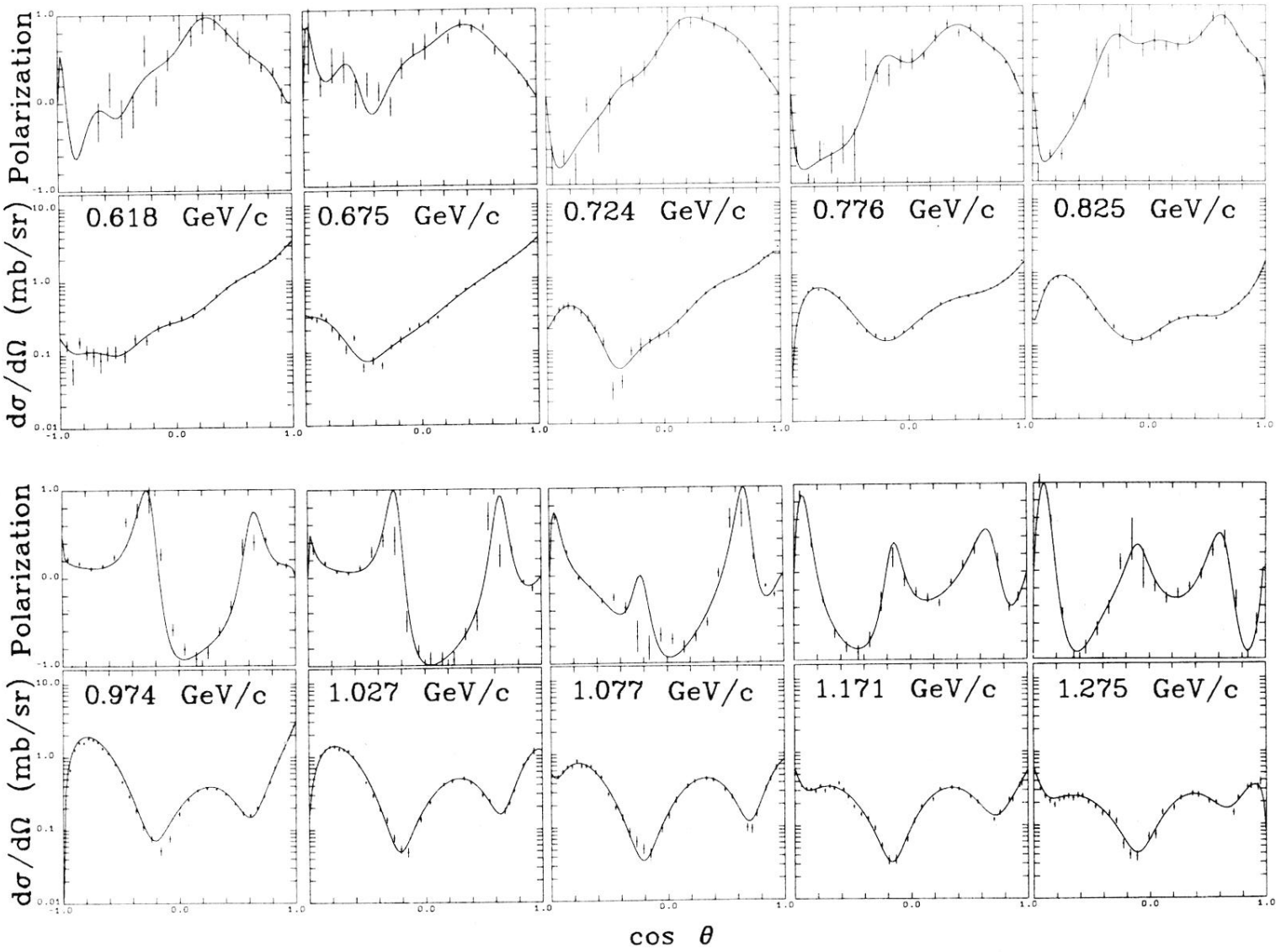

FIG. 6. B76 data and $N = 10$ polynomial representation thereof.

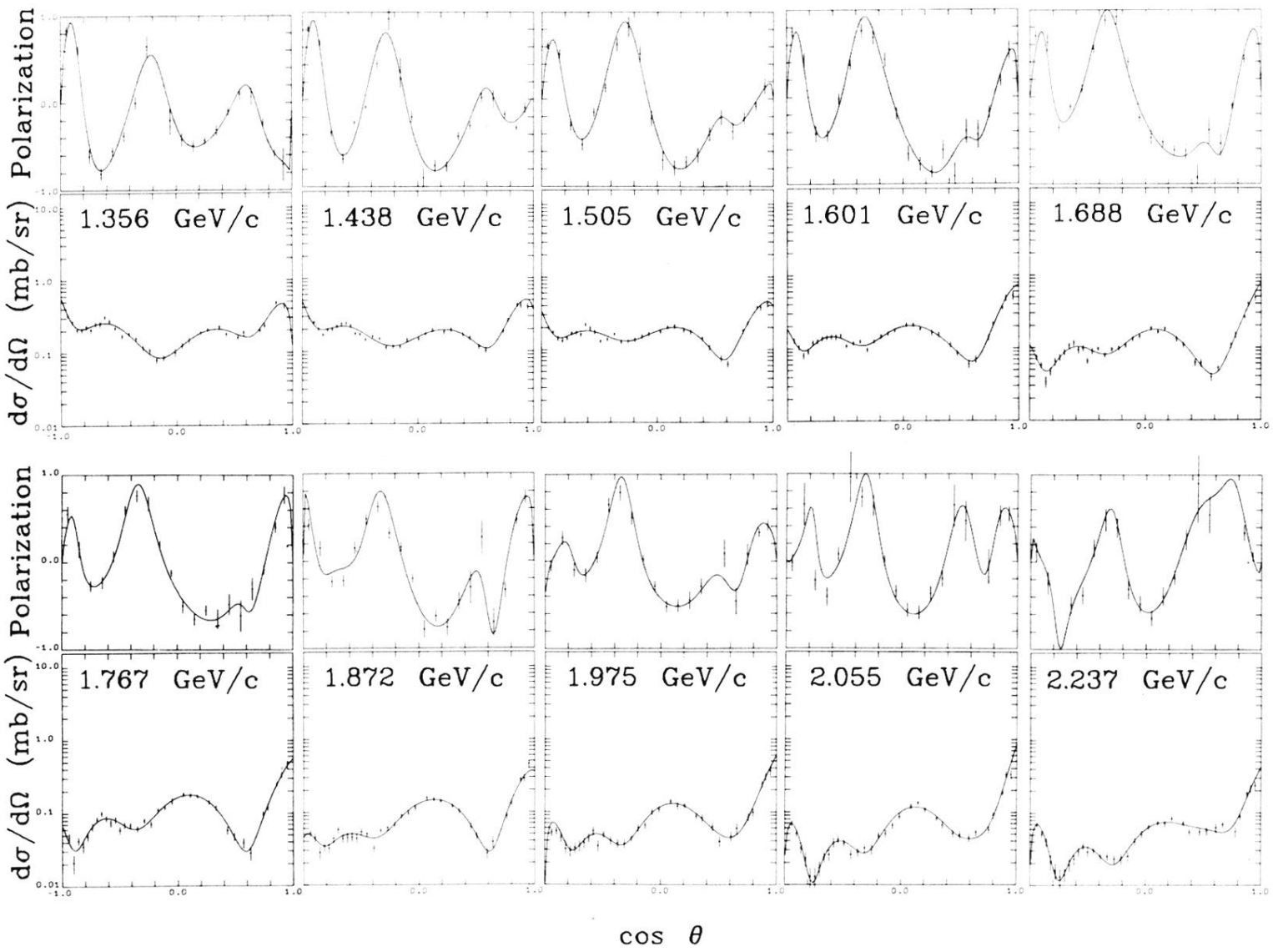

FIG. 6. (*continued*)

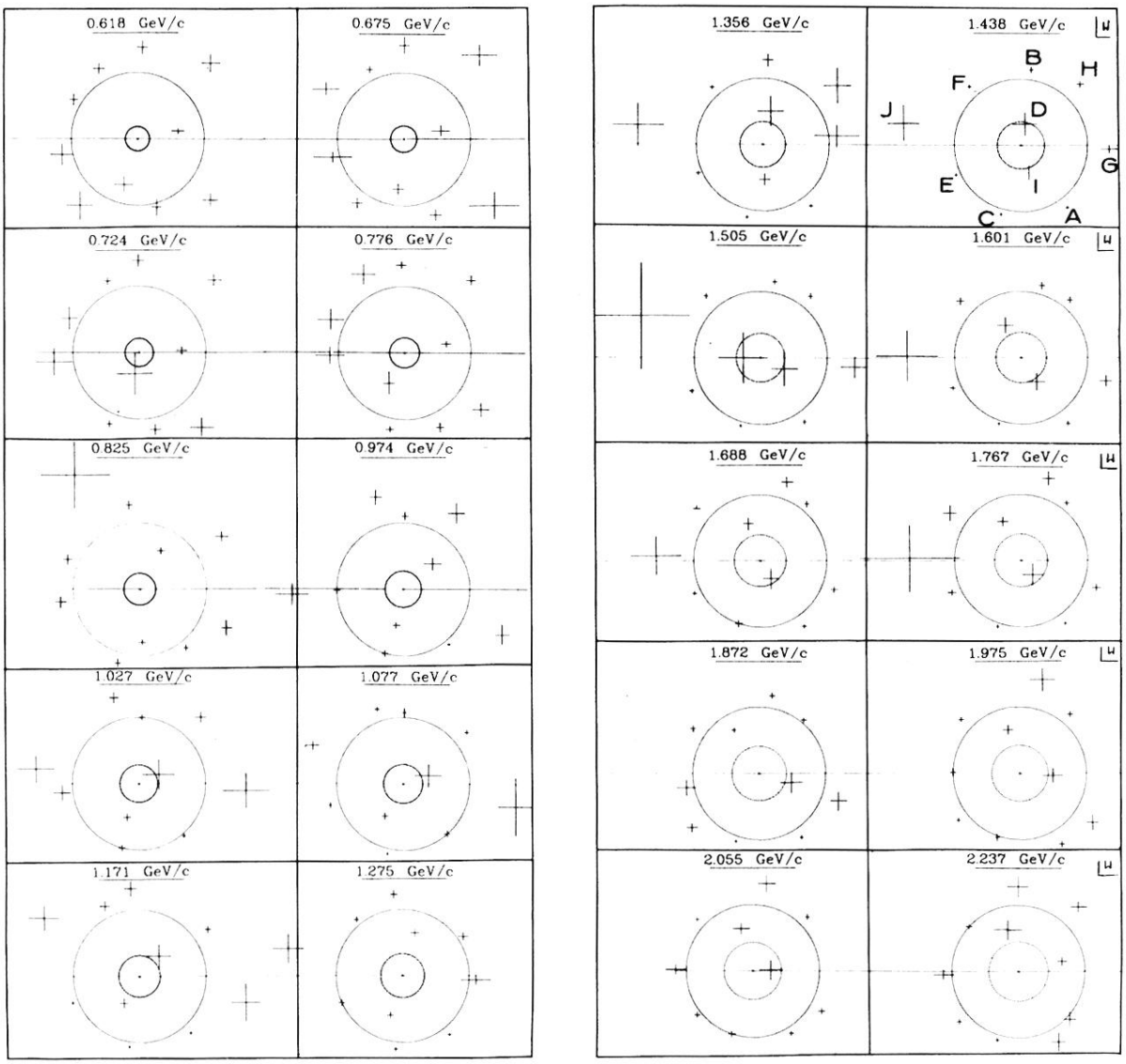

FIG. 7. Location of the zeros of the 10th-order polynomial fit in the w plane for the 20 energies of the B76 data.

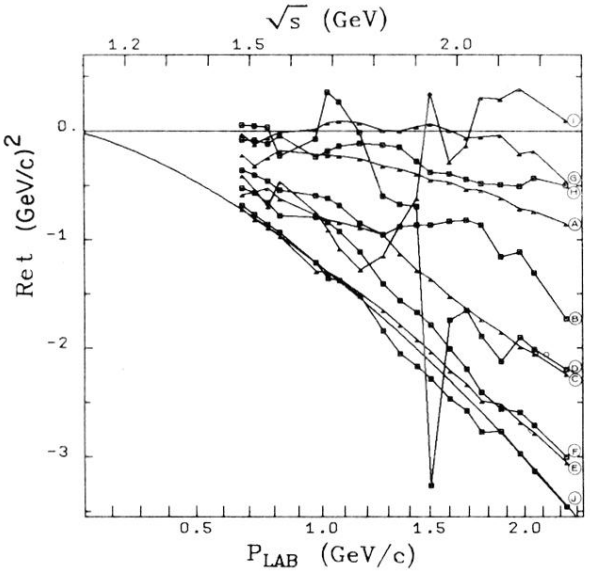

FIG. 8. Ret versus $\sqrt{s}$ and p_{lab}.

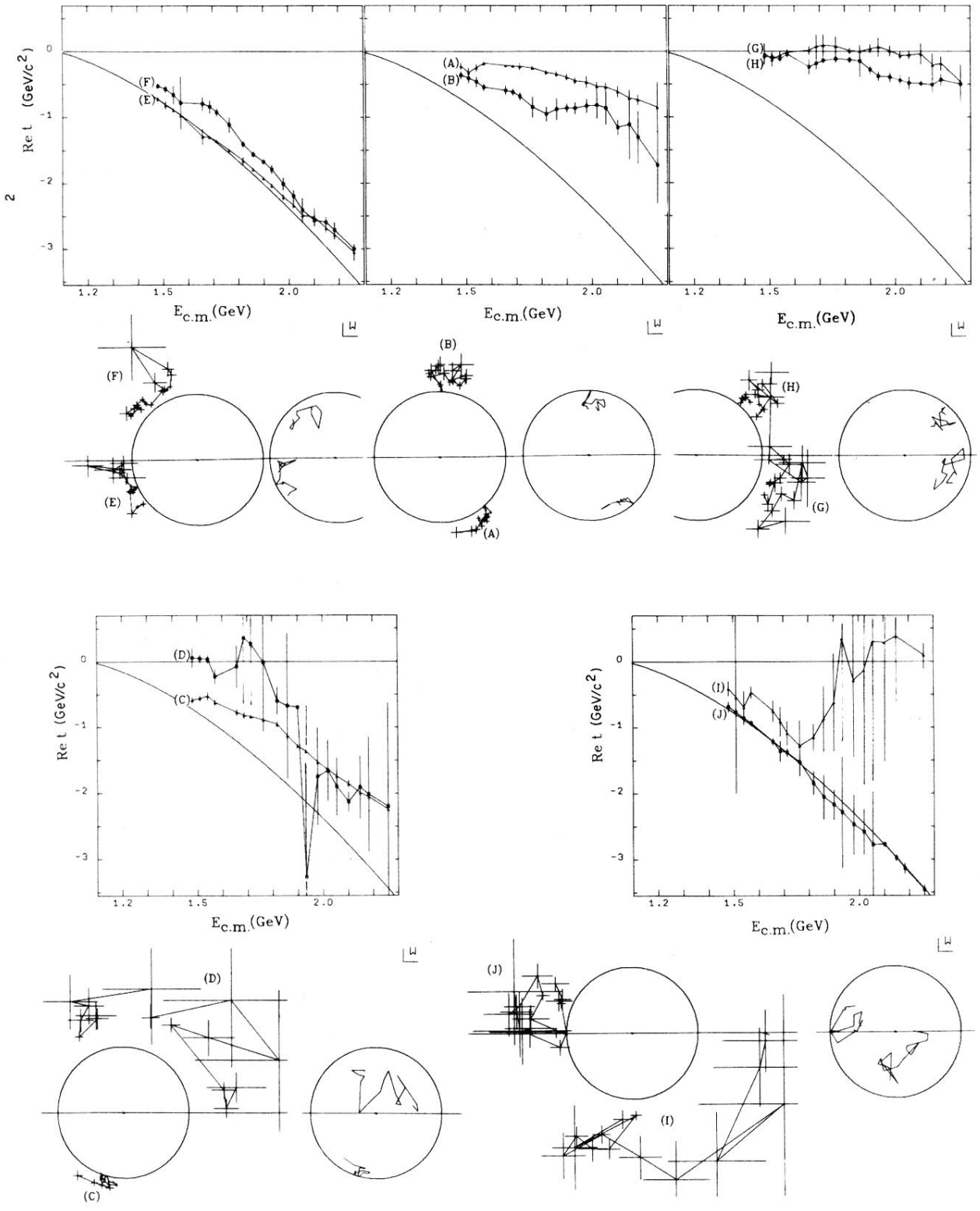

FIG. 9. Detail of Fig. 8 with errors and corresponding location of the trajectories in the w plane, either outside (with errors on the zero position) or inside the unit circle.